ornl

NUREG/CR-4346
ORNL/TM-9479

OAK RIDGE
NATIONAL
LABORATORY

MARTIN MARIETTA

Aerosol Release Experiments in the Fuel Aerosol Simulant Test Facility: Undersodium Experiments

J. C. Petrykowski
A. W. Longest
J. M. Rochelle
A. L. Wright

Prepared for the U.S. Nuclear Regulatory Commission
Office of Nuclear Regulatory Research
Under Interagency Agreements DOE 40-551-75 and 40-552-75

OPERATED BY
MARTIN MARIETTA ENERGY SYSTEMS, INC.
FOR THE UNITED STATES
DEPARTMENT OF ENERGY

Printed in the United States of America. Available from
National Technical Information Service
U.S. Department of Commerce
5285 Port Royal Road, Springfield, Virginia 22161
NTIS price codes—Printed Copy: A04 Microfiche A01

NUREG/CR-4346
ORNL/TM-9479
Dist. Category R7

Engineering Technology Division

AEROSOL RELEASE EXPERIMENTS IN THE FUEL AEROSOL SIMULANT TEST FACILITY: UNDERSODIUM EXPERIMENTS

J. C. Petrykowski
A. W. Longest
J. M. Rochelle
A. L. Wright

Manuscript Completed — August 7, 1985
Date Published — September 1985

NOTICE: This document contains information of a preliminary nature. It is subject to revision or correction and therefore does not represent a final report.

Prepared for the
U.S. Nuclear Regulatory Commission
Office of Nuclear Regulatory Research
under Interagency Agreements DOE 40-551-75 and 40-552-75

NRC FIN No. B0121

Prepared by the
OAK RIDGE NATIONAL LABORATORY
Oak Ridge, Tennessee 37831
operated by
MARTIN MARIETTA ENERGY SYSTEMS, INC.
for the
U.S. DEPARTMENT OF ENERGY
under Contract No. DE-AC05-84OR21400

CONTENTS

NOMENCLATURE

C	Speed of sound in sodium, m/s
E	Electrical energy delivered to sample during capacitor discharge, J
h	Pool level referenced to centerline of vaporizer, mm
M	Mach number of bubble-driven pool flow
P	Pressure, Pa
P_{CG}	Cover gas pressure, Pa
P_D	Dynamic pressure in pool, Pa
P_S	Static pressure in pool, Pa
q	Local flow speed in pool, m/s
q_B	Speed of the bubble interface, m/s
R	Radius of equivalent spherical bubble, mm
r	Radial coordinate measured from center of bubble, mm
t	Time after capacitor discharge; s in Eq. (2), ms in Eq. (6c)
V_B	Bubble volume, mm^3
V_{CG}	Cover gas volume, mm^3

Greek

γ	Aerosol release parameter; bubble kinematics parameter
$\frac{\partial \phi}{\partial r}$	Velocity field for potential flow, m/s
κ	Specific heat ratio
ρ	Mass density, kg/m^3
$\rho \frac{\partial \phi}{\partial t}$	Impulse pressure, Pa
ϕ	Velocity potential, m^2/s

Subscripts

CG	Cover gas
MAX	Maximum value
o	Baseline value

AEROSOL RELEASE EXPERIMENTS IN THE FUEL AEROSOL SIMULANT TEST FACILITY: UNDERSODIUM EXPERIMENTS

J. C. Petrykowski
A. W. Longest
J. M. Rochelle
A. L. Wright

ABSTRACT

The release of uranium dioxide (UO_2) aerosols from pools of sodium was studied in a series of ten experiments in the Fuel Aerosol Simulant Test (FAST) facility at Oak Ridge National Laboratory. The experiments were designed to provide a mechanistic basis for evaluating the radiological source term associated with a postulated, hypothetical core-disruptive accident (HCDA) in a liquid-metal fast breeder reactor (LMFBR). Aerosol was generated by capacitor discharge vaporization of UO_2 pellets that were submerged in a sodium pool under an argon cover gas. Measurements of the pool and cover gas pressures were used to study the transport of aerosol contained by vapor bubbles within the pool. Cover gas samples were filtered to determine the quantity of aerosol released from the pool. Trace amounts of UO_2 aerosol (<0.3% of the total pellet mass) were detected in the cover gas samples suggesting that the bulk of aerosol was trapped within bubbles confined by the pool. The report contains (1) a description of the experiments; (2) data records for the pool pressure, the cover gas pressure, and the UO_2 aerosol concentration in the cover gas; and (3) an analysis of the experimental findings using simplified models of bubble behavior.

---

1. INTRODUCTION

1.1 Overview

This report summarizes experiments conducted in the Fuel Aerosol Simulant Test (FAST) facility to study the transport and release of uranium dioxide (UO_2) aerosols from pools of sodium.[1-4] These out-of-reactor experiments were designed within the Aerosol Release and Transport (ART) Program at Oak Ridge National Laboratory (ORNL) to provide a data base for mechanistic assessments of the primary source term associated with a hypothetical core-disruptive accident (HCDA) in liquid-metal fast breeder reactors (LMFBRs). A series of ten experiments was conducted from June 1983 through April 1984 in which UO_2 pellets were energized in sodium pools using a capacitor discharge vaporization (CDV) technique to produce aerosols of a type that might exist following an HCDA. The experimental data were analyzed to determine the conditions under which UO_2 aerosols could be released from a sodium pool. Financial

support was provided by the Division of Accident Evaluation of the U.S. Nuclear Regulatory Commission. This report completes the principal objectives of the program[5] and complements reports of Wright et al.[6,7] describing preliminary CDV experiments using both water pools and argon atmospheres.

1.2 Experimental Objectives

Development of meaningful out-of-reactor source term experiments was predicated on a phenomenological understanding of HCDAs. Two types of energetic HCDAs have been postulated to release fuel, fission products, and sodium vapor from LMFBR cores: transient undercooling with failure to scram (TUC) and transient overpower (TOP). A TUC could be initiated by a coolant flow coastdown followed by heatup and local boiling of core coolant. In a TOP, a reactivity insertion caused by rapid withdrawal of the control rods leads to fuel pin failure and mixing of molten fuel and coolant. Positive reactivity feedback in both accidents caused by sodium voiding produces a rapid power excursion and vaporization of portions of the core. The excursions terminate when the internal core pressures are sufficient to produce mechanical disassembly. Although the fuel energy density is determined by complex reactivity feedback mechanisms, the power excursions can be characterized by a "slow" deposition ramp (predisassembly) followed by a "rapid" deposition ramp (disassembly).[5,8]

To simulate these transients in the FAST facility, UO_2 samples were energized by Joule self-heating. Usually, the sample was pressurized with xenon and submerged in a sodium pool under an argon cover gas. Energy was input during the "predisassembly" phase by a power supply operated in a stepwise-constant power mode. At the end of preheat, the sample was partially molten with an energy density of ~1 kJ/g. Energy stored in capacitor banks was then discharged in a few milliseconds to vaporize and "disassemble" the sample.[9,10] Surrounded by liquid sodium, a multiphase mixture of UO_2 and xenon formed the contents of the so-called "bubble." Fragmentation and condensation within the bubble produced aerosols of UO_2 during and after disassembly. Bubble kinematics governed whether aerosols were released to the cover gas. Pressures in the cover gas and pool were measured to reveal the size of the submerged bubble and flow characteristics of the pool. Gas sampling techniques were used to measure the amount of aerosol suspended in the cover gas.

2. DESCRIPTION OF EXPERIMENTS

2.1 Experimental Facility

The FAST facility consists of (1) the FAST vessel and associated hardware and measurement equipment, (2) the vaporizer unit in which the UO_2 sample was initially contained, (3) a preheater and capacitor bank power supply system used to energize the sample, and (4) the control room. The FAST vessel and measurement equipment are shown schematically in Fig. 1. The vessel is ~1.83 m high and ~0.61 m in outer diameter and has an internal volume of ~0.46 m^3. The vessel was fabricated from 0.022-m-thick 304 H stainless steel and has a removable head. The design temperature limit of the vessel is 880 K; the design pressure limit is 3.08 MPa. Electric heaters attached to the vessel were used to maintain an operating temperature of ~800 K.

The vaporizer unit, shown schematically in Fig. 2, includes the electrodes, the test sample, and sample holders, which provided electrical and mechanical connections to the sample. The test sample consisted of 13 UO_2 pellets (4.85-mm diam) stacked end-to-end having a total mass

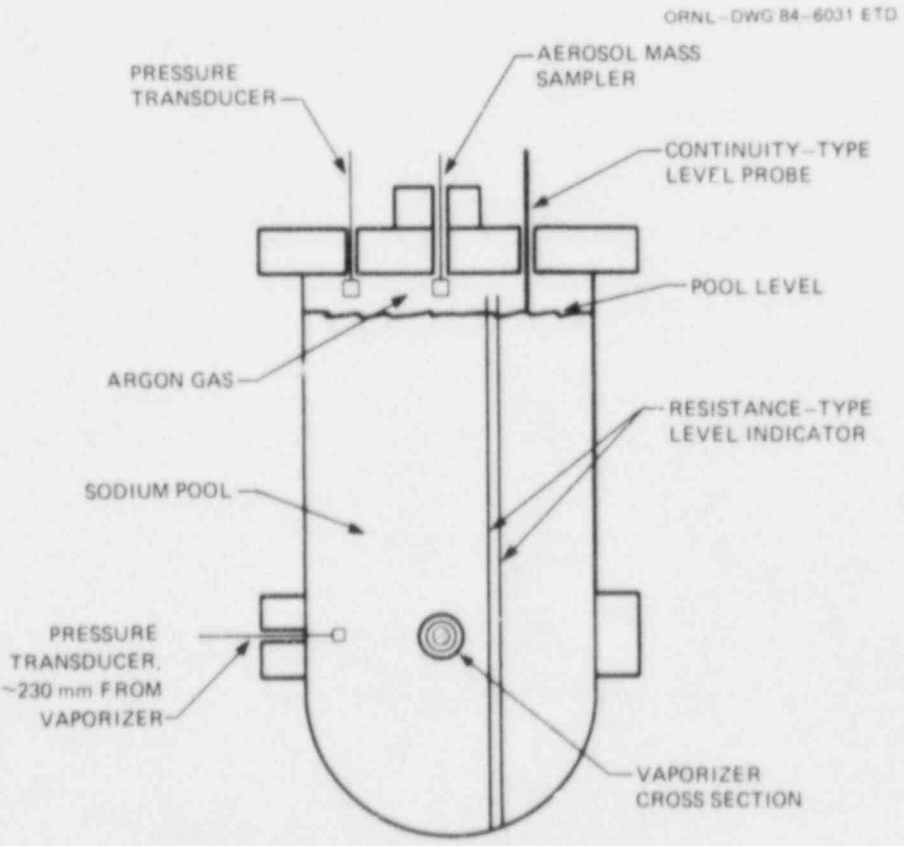

Fig. 1. Simplified schematic of FAST vessel.

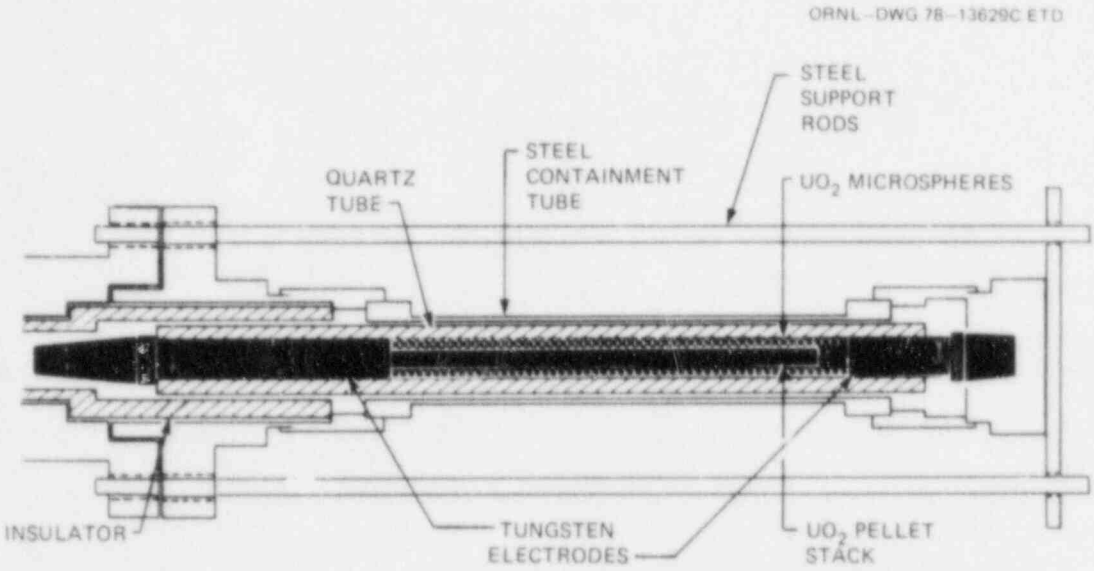

Fig. 2. FAST vaporizer unit schematic.

of ~17.3 g and an overall length of ~90 mm. The pellet stack was surrounded by ~32 g of UO_2 microspheres (300- to 500-μm diam) that were used to thermally insulate the pellets. Electrical contact with the power supply was maintained through electrodes at the ends of the pellet stack. Pellets and microspheres were contained in a quartz tube surrounded by a steel tube. The gap between the tubes and the void space between microspheres were pressurized with xenon to simulate fission gases. Axial and circumferential grooves were inscribed on the steel tube to provide fracture sites for efficient rupture during the capacitor discharge.

The power supply system consists of a power-controlled preheater, capacitor banks, electrical connections to the vaporizer unit, and switching and control circuitry. Electric power delivered to the sample from the preheater and capacitor banks was converted to thermal energy by Joule self-heating. The preheater was used to lower the electrical resistance of the sample by several orders of magnitude to enable a very rapid (~2-ms) capacitor discharge.[11] Four capacitor banks containing ten capacitors each were fired simultaneously on a predetermined signal. Total bank capacity is 180 kJ at 2500 V, although 1950-V settings were usually selected for these experiments. Power levels typically reached ~1.6 kW during preheat and ~10 MW during discharge.

Experimental control and data recording were performed in the control room.

2.2 Measurement of Experimental Parameters

2.2.1 Preheat measurements

Measurements were made of the electric power, voltage drop, and electric current supplied to the sample. During preheat, an ac power supply was used, and constant power levels were maintained by conduction

angle control (phase firing) of inverse-parallel silicon-controlled rectifiers.[12] Because voltage and current were in phase, measurement of the peak values was used to calculate the sample resistance at specified preheat power levels.

The power input and resistance data were used to compute a corresponding steady state temperature distribution in the sample.[13] An iterative, finite difference technique was used to calculate heat transfer in a pellet stack surrounded by microspheres. Joule heating is represented by a distribution of heat sources; the total heat released by these sources must balance the heat loss by radiation from the outermost microspheres. Figure 3 shows the predicted distribution for a preheat power level of 1600 W and suggests that partial melting occurred for these conditions. This conclusion was supported by Wright's preheat-only experiment.[11] The internal energy of the sample at the end of preheat could be determined from the temperature distribution and published thermophysical data.[14]

2.2.2 Capacitor discharge measurements

The circuit for the CDV system is illustrated in Fig. 4. During capacitor discharge, measurements were made of the circuit current and

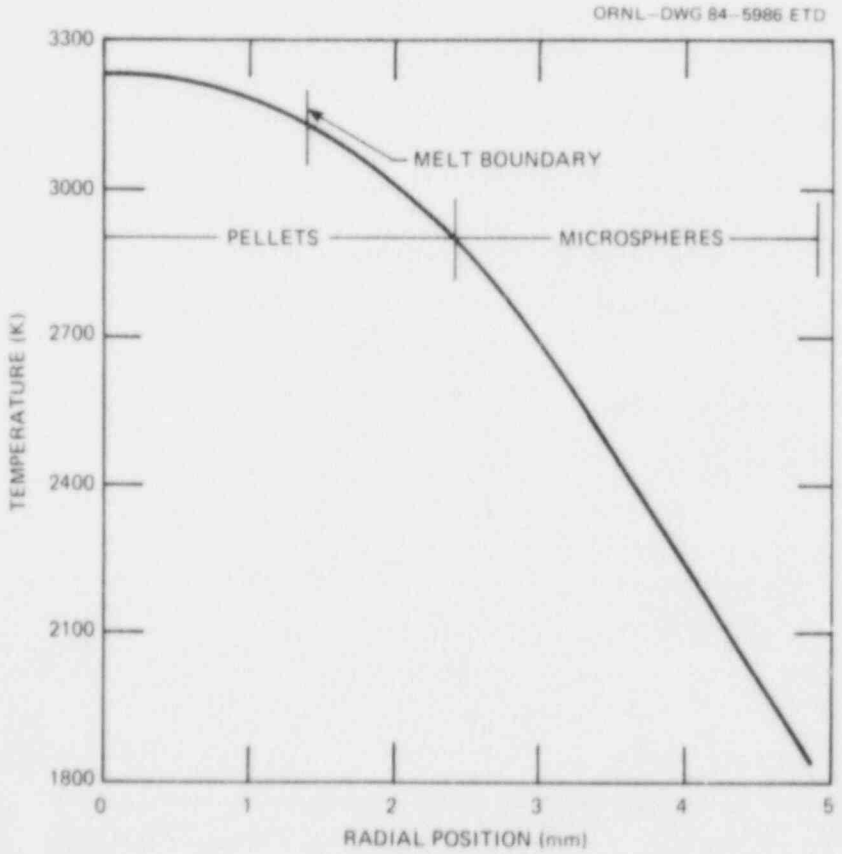

Fig. 3. Calculated temperature distribution in UO_2 pellets and microspheres following 1600-W preheat.

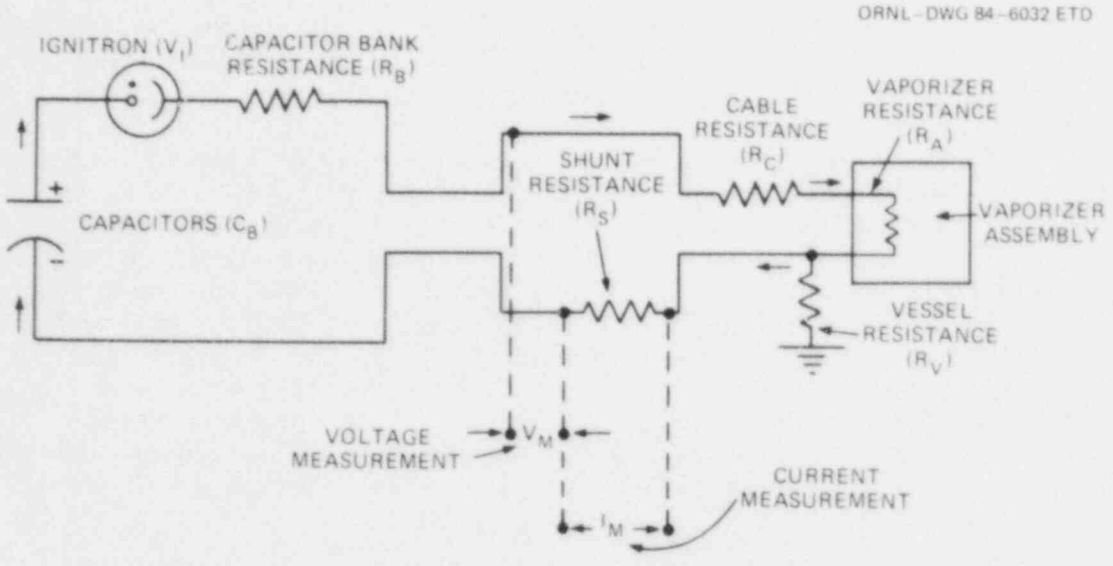

Fig. 4. Simplified schematic diagram of the capacitor discharge vaporization system.

voltage drop across the test sample, cables, and shunt as a function of time after the start of capacitor discharge. These data were recorded using an oscilloscope that digitized analog input data as rapidly as 0.5 μs/point. Using a recording rate of 10 μs/point, a 10-ms record of capacitor discharge voltage and current was obtained in each experiment.

An example of the recorded capacitor discharge voltage and current data is shown in Fig. 5. The figure shows that the current rose sharply at 2.95 ms after the start of capacitor discharge, which was interpreted

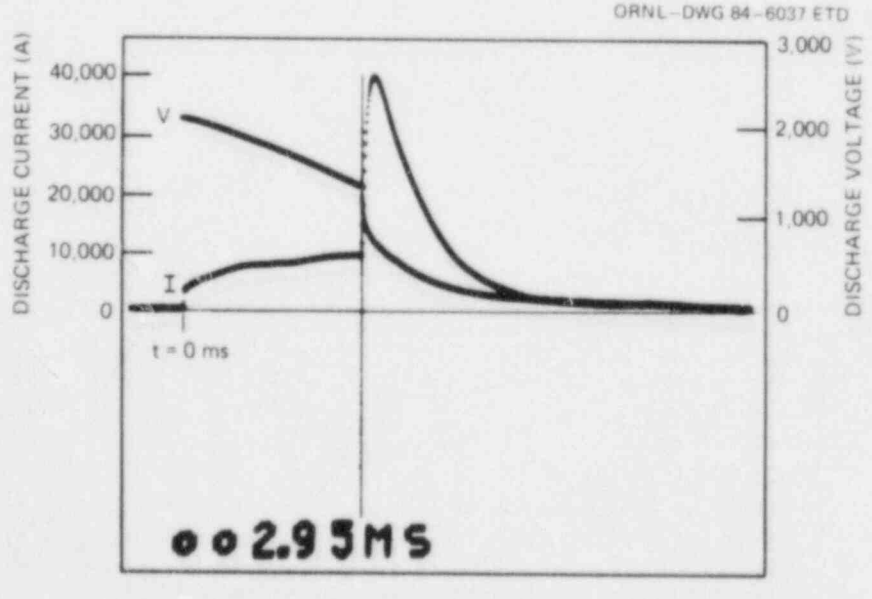

Fig. 5. Measured voltage and current during typical capacitor discharge vaporization sequence (FAST-113).

as a current shunt between the high-voltage electrode and ground. This occurred when sufficient UO_2 vapor was evolved to overpressurize and rupture the quartz and steel tubes and disassemble the sample. The voltage and current data were used to calculate the energy input to the sample caused by Joule heating, assuming that no significant energy input occurred after shorting began. This "CDV energy input" was calculated by time integrating the voltage-current product using the trapezoidal rule. Estimates of the peak energy density of the sample were made by adding the "CDV energy input" to the internal energy of preheat. As an example, the peak energy density in FAST-104 was estimated to be ~2.8 kJ/g.

2.3 Thermomechanical Measurements

2.3.1 Pressure measurements

As the sample disassembled, a dynamic multiphase mixture was formed containing UO_2 vapors and solids, xenon, and possibly steel, quartz, and sodium. Pressures resulting from heat, mass, and momentum transfer between the mixture and the surrounding media were measured using two Kaman Sciences pressure transducers. One transducer was positioned radially 0.23 m from the vaporizer assembly; the other was positioned axially above the vaporizer assembly near the top of the vessel. In all but one experiment (FAST-111), the sodium pool covered the vaporizer and the submerged mixture formed a bubble. The radially and axially mounted transducers measured the pool and cover gas pressure, respectively. Cover gas pressure measurements were also used to estimate the size of the bubble as a function of cover gas compression.

Pressure data were recorded using a Nicolet Explorer III digital oscilloscope. Pressure-time traces for each experiment are presented in Sect. 3. An interpretation of this data will be presented in Sect. 4 of this report.

2.3.2 Liquid level measurements

The level of the sodium pool was adjusted in each experiment to vary the distance between the vaporizer and the cover gas. Because this distance was roughly equivalent to the distance that a submerged aerosol particle must travel before entering the cover gas, precise liquid level measurements were needed. An electrical resistance-type meter measured levels to within an estimated ±3 cm uncertainty in experiments 104–112. A more accurate, electrical continuity probe was used in FAST 113 because the desired liquid level (30 mm) fell within the uncertainty range of the resistance device.

2.4 Aerosol Measurements

Aerosol mass concentration measurements in the cover gas were made using an eight-stage mass sampler. This sampler was installed in a port

at the top of the vessel and was connected to eight, 3-L, pre-evacuated sampling bottles. The sampling procedure measured both the amount of argon cover gas drawn through an aerosol collection filter (located in the cover gas space) and the amount of material trapped by the filter. Sintered stainless steel (Type 316) filters measuring 28.5-mm diam by 1.6 mm thick with a 2-μm pore size were used. The filters were analyzed for uranium using a fluorometric technique and for sodium, silicon, iron, and 28 other species by inductively coupled plasma spectrometry. The amount of aerosol transported to the cover gas and the rate at which depletion occurred were determined from this data.

2.5 FAST Experimental Procedures

Each of the FAST experiments followed the same procedures. While maintaining an argon purge through the vessel, the vaporizer unit and aerosol sampling equipment were loaded into the vessel. The vessel was evacuated to remove air and then backfilled with argon to provide an inert environment for the sodium. Sodium holding tanks and plumbing were heated above the sodium melting point so that liquid sodium flow could be maintained. Transfer of sodium to the vessel was achieved by applying argon pressure to the tanks while fill-and-drain valves were open. After transfer was completed, the vessel was further pressurized with argon and heated slowly over a 24-h period to an operating temperature of ~800 K. As this temperature was approached, heater settings were gradually lowered to establish a steady state temperature distribution. Final adjustments were made to the liquid level and argon cover gas and xenon sample pressures to account for thermal effects during heatup. The pool and cover gas pressure transducers were calibrated in situ, and the capacitor discharge system was checked. After this check was completed, the vaporizer assembly was connected to the preheat and capacitor discharge system.

Preheating of the sample began at low-power levels and increased in prescribed increments until a steady state temperature distribution was achieved at 500 to 600 W. Capacitor banks were charged to 1950 V in preparation for firing. After a final check of all systems was completed, the firing system was placed in an automatic mode. This mode consisted of a high-power level (1600 W) preheat lasting 28 s, a 2-s delay for local thermal equilibration, and, finally, capacitor bank firing. Aerosol sampling in the cover gas commenced 1 to 2 min after firing and continued for nearly 1 h at intervals of 2 to 15 min.

During each experiment, pressure and electrical data from preheat and capacitor discharge were collected. The capacitor discharge data were stored in a PDP/8A computer, which was used to calculate the energy input from capacitor discharge. Pressure transducer data were stored on the "minifloppy" disk storage system built into the Explorer III storage oscilloscope. Photographs of the oscilloscope traces of the capacitor discharge data and pressure transducer data were taken after each experiment. Hard disk files containing raw pressure transducer data were created on the DEC-10 computer for archival and plotting purposes. After data were recorded, the sodium was drained from the vessel into the holding tanks, and heating was terminated to allow the vessel to cool to ambient temperature (~60 h required for cooldown).

3. EXPERIMENTAL DATA RECORDS

3.1 Experimental Test Plan

The FAST experiments were conducted using a variety of argon and xenon pressures and sodium pool levels to determine what effect these parameters had on aerosol release to the cover gas. It was assumed that the pool level was the most critical experimental parameter affecting release because it alone accounts for the physical extremes: no release, corresponding to an infinitely high level, and total release, corresponding to subvaporizer levels. For this reason, pool level settings spanned a wide range of values (−300 to +1060 mm) with increased selectivity at low, "positive" levels. Argon pressure was varied to determine the effect of cover gas compressibility on bubble sizes, pool dynamics, and aerosol release; xenon pressure selectivity gaged the sensitivity of aerosol release to noncondensible carrier gas content. Both pressures were varied by factors of 2.5 during the course of the experiments. An outline of the experimental test plan showing nominal conditions appears in Table 1. Actual experimental conditions are listed in Table 2.

3.2 Control of Other Experimental Factors

Variations in the electrical and mechanical characteristics of the vaporizer assembly made it difficult to evaluate vaporizer performance a priori. Performance was estimated by calculating the amount of electrical energy that was delivered to the sample during capacitor discharge. Assuming delivery ceased when shorting occurred, "energy input" was determined by time integrating the power input rate (voltage-current product). Factors affecting the input rate and the "shorting time" were the electrical resistance of the sample and the ultimate burst pressure of the vaporizer assembly.

Differences in the measured electrical resistance of vaporizer assemblies were probably caused by variations in: (1) pellet stack alignments, (2) preheat temperature levels, and (3) intra-assembly contact resistances. Burst pressure variations were attributed to differences in: (1) quality control of quartz and/or steel tube fabrication processes and (2) diametral clearances between the quartz tube and tungsten electrodes. Physical dimensions of vaporizer components are listed in Table 3.

Electrical measurements of vaporizer performance are listed in Table 4 and show that changes in "CDV energy input" were primarily caused by variations in shorting time. For example, low energy input observed in FAST-108 and -109 was attributed to early shorting of the vaporizer.

This tendency was reversed in subsequent experiments by decreasing preheat power levels to obtain lower sample temperatures and electrical conductivities at the start of discharge. These changes accounted for slower, more sustained power input, more uniform heating of the sample, and delayed shorting of the assembly.

Table 1. FAST experimental test plan[a]

Experiment No.	Pressure [kPa (abs)]		Nominal[b] sodium pool level above vaporizer centerline (mm)	Objective
	Argon cover gas	Xenon sample		
FAST-104	120	135	1070	Repeat of FAST 103 Compare with previous results
FAST-105	120	340	1070	Determine effect of changing xenon pressure
FAST-106	120	340	200	Determine effect of changing pool level
FAST-107	120	340	100	Same as 106
FAST-108	120	340	50	Same as 106
FAST-109	300	340	50	Determine effect of changing pool level at a second cover gas pressure level
FAST-110	300	340	100	Same as 109
FAST-111	120	340	−300	Determine aerosol behavior over sodium at 810 K Verify aerosol sampling technique
FAST-112	300	340	200	Same as 109
FAST-113	300	340	30	Same as 109

[a]In all tests, the nominal temperatures of the vessel and the sodium were 810 K.

[b]See Table 2 for actual pool levels.

Table 2. Experimental conditions

Experiment No.	Type	Temperature (K)	Argon cover gas		Sample pressure at start of low preheat [kPa (abs)]	Sodium pool	
			Volume (m^3)	Pressure [kPa (abs)]		Volume (m^3)	Level above vaporizer centerline (mm)
FAST-103[a]	Undersodium	810	0.092	120	134	0.37	1050
FAST-104	Undersodium	810	0.090	120	133	0.37	1060
FAST-105	Undersodium	810	0.095	120	341	0.37	1040
FAST-106	Undersodium	810	0.30	120	340	0.16	240
FAST-107	Undersodium	810	0.32	121	341	0.14	140
FAST-108	Undersodium	810	0.34	120	340	0.12	80
FAST-109	Undersodium	810	0.33	300	341	0.13	100
FAST-110	Undersodium	810	0.32	300	340	0.14	140
FAST-111	Oversodium	810	0.45	122	341	0.014	−300
FAST-112	Undersodium	810	0.30	300	338	0.16	250
FAST-113	Undersodium	810	0.35	119	338	0.11	30

[a]Included for comparison. FAST-103 was performed on December 15, 1981, prior to a 1-year shutdown of the facilities.

Table 3. UO_2 specimen data

Experiment No.	UO_2			Quartz tube dimension (mm)	
	Pellet stack		Microsphere mass (g)	Inside diameter	Outside diameter
	Mass (g)	Length (mm)			
FAST-103[a]	17.36	90.4	32.93	9.70	17.15
FAST-104	17.58	91.7	32.39	9.70	17.15
FAST-105	17.49	91.2	32.06	9.70	17.15
FAST-106	17.59	91.4	31.97	9.70	17.15
FAST-107	17.50	91.1	31.48	9.70	17.15
FAST-108	17.36	90.3	31.68	9.70	17.15
FAST-109	17.66	91.9	31.86	9.70	17.15
FAST-110	17.63	91.5	32.08	9.70	17.15
FAST-111	17.57	91.5	31.99	9.73	17.15
FAST-112	17.44	90.7	31.84	9.73	17.15
FAST-113	17.36	91.1	31.70	9.70	17.15

[a]Included for comparison. FAST-103 was performed on December 15, 1981, prior to a 1-year shutdown of the facilities.

Table 4. Electrical energy input data

Experiment No.	Preheat power[a] (W)		Resistance at end of high preheat (Ω)	Time delay between high preheat and CDV (s)	Energy stored in capacitor banks (kJ)	CDV time to shorting (ms)	CDV energy input (kJ)
	Low	High					
FAST-103[b]	600	1600	0.43	2.0	76.5	3.15	37.9
FAST-104	600	1600	0.44	2.0	76.5	3.14	37.4
FAST-105	600	1600	0.41	2.0	76.9	2.61	32.2
FAST-106	600	1600	0.41	2.0	76.9	2.98	37.6
FAST-107	600	1600	0.46	2.0	76.5	2.30	28.8
FAST-108	600	1600	0.39	2.0	76.9	1.55	19.6
FAST-109	600	1600	0.40	2.0	76.5	1.65	20.3
FAST-110	540	1600	0.40	2.0	76.5	2.35	28.2
FAST-111	500	1550	0.41	2.0	77.3	1.93	22.8
FAST-112	540	1600	0.40	2.0	76.5	2.16	26.5
FAST-113	540	1600	0.41	2.0	76.5	2.95	37.0

[a]Preheat power levels modified for FAST-110 through FAST-113 to improve vaporizer performance.

[b]Included for comparison. FAST-103 was performed on December 15, 1981, prior to a 1-year shutdown of the facilities.

3.3 Reproducibility of Experimental Conditions

Control of FAST experimental conditions was measured by the degree to which experimental results could be reproduced using similar operating conditions. Using this hypothesis, experimental control was evaluated by selecting conditions for the first experiment, FAST-104, that were almost identical with Wright's preliminary undersodium experiment,[7] FAST-103 (see Tables 2 and 4). Comparison of controlled experimental conditions (i.e., gas pressures, pool levels, and preheat power levels) revealed <3% variation between the two experiments. The resulting capacitor discharge parameters (i.e., discharge times and energies) varied by <2%. The measured pool pressures following capacitor discharge were also very similar. Figure 6 shows a superposition of the measured pool pressure data. The pressure curves exhibit similar shape and orientation and, with the third spike on FAST-103 excluded, would be difficult to differentiate with the unaided eye. These observations suggest that adequate experimental control was possible and that experimental results could be replicated to a satisfactory degree.

3.4 Pool and Cover Gas Pressure Data

Data records of the pool pressure and cover gas pressure are plotted as functions of time in Figs. 7–16. Each record covers the first 100 ms of an experiment; this period includes capacitor discharge, vaporizer disassembly, and much of the ensuing hydrodynamic interactions. The first data point in each record was synchronized with capacitor bank firing. A pool pressure record was not obtained for FAST-111 because the pool level was below the access port used for inserting the pool pressure transducer. Baseline cover gas pressures are noted in the figure captions; the pressure unit is kilopascals (kPa) absolute.

3.5 Aerosol Data

The total mass of uranium aerosol in the cover gas is plotted vs time in Figs. 17 and 18 for experiments conducted with cover gas pressures of 120 and 300 kPa, respectively. These data are presented so that aerosol release can be estimated in absolute (total mass) and relative (concentration) terms. Concentration is determined by dividing the total mass by the total cover gas volume. Both measures account for depletion of cover gas that occurred as a result of sampling.[2,3]

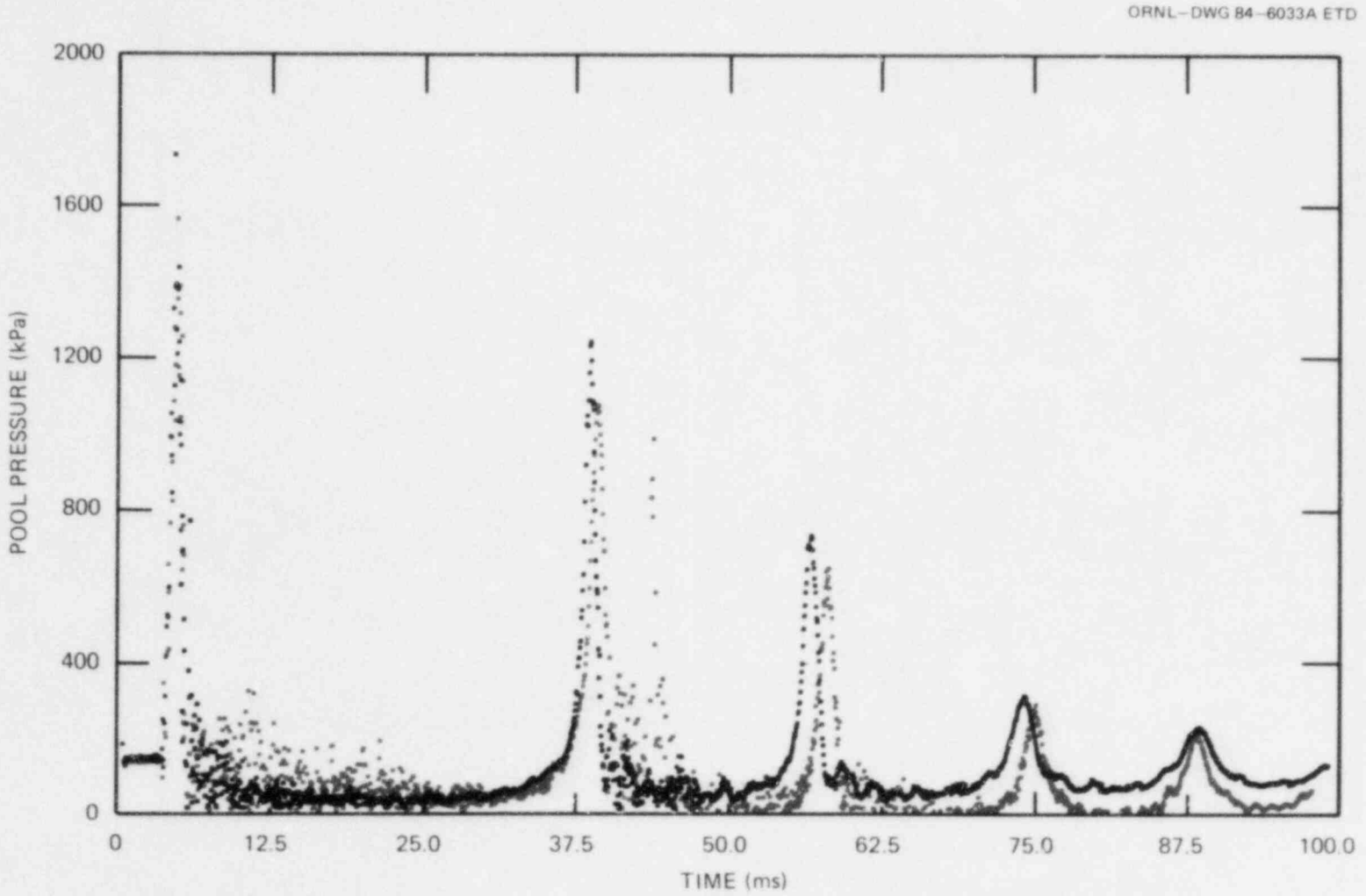

Fig. 6. Comparison of measured pool pressures [FAST-103 (red), FAST-104 (black)].

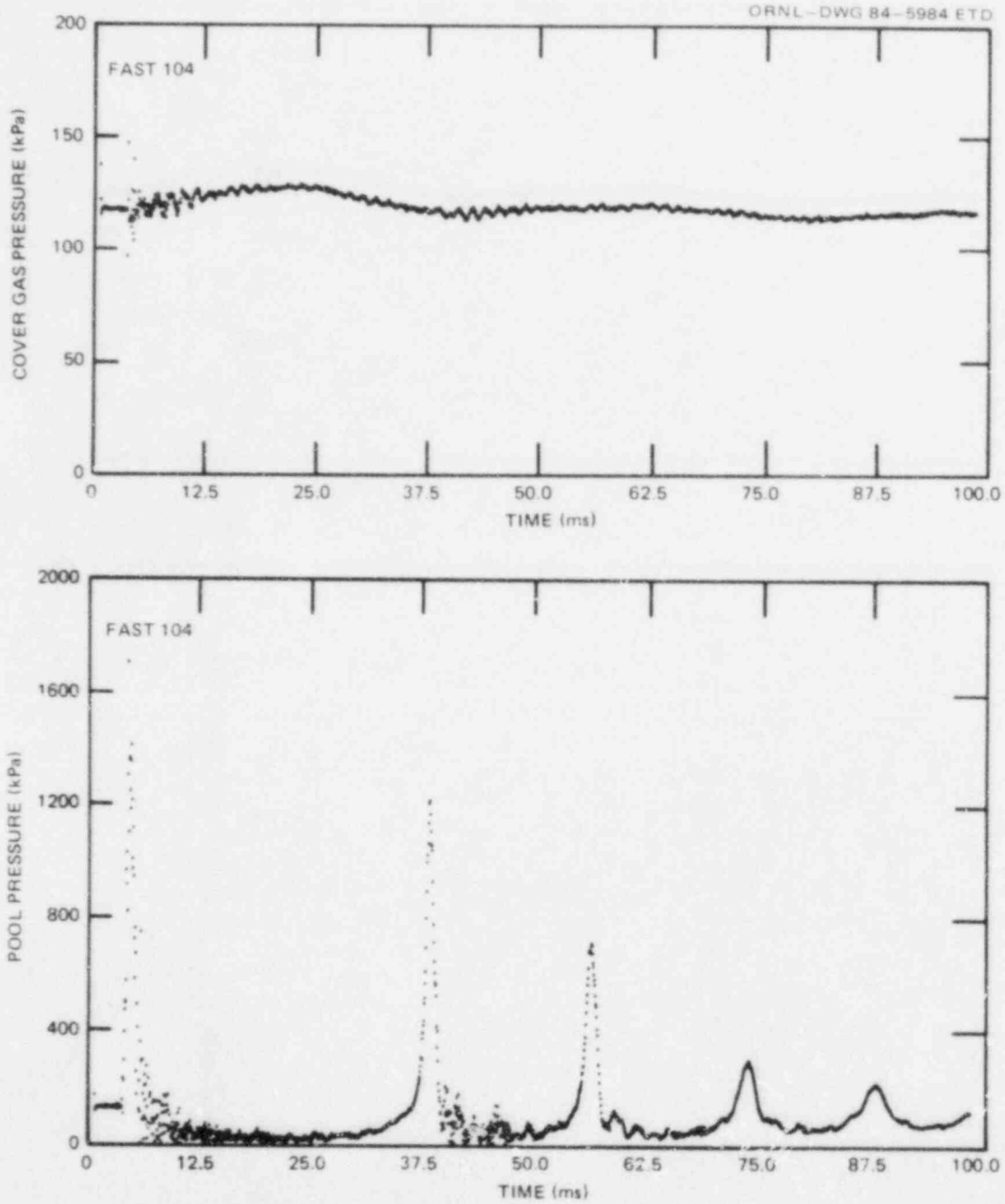

Fig. 7. Measured pressures, FAST-104 (baseline cover gas pressure is 120 kPa).

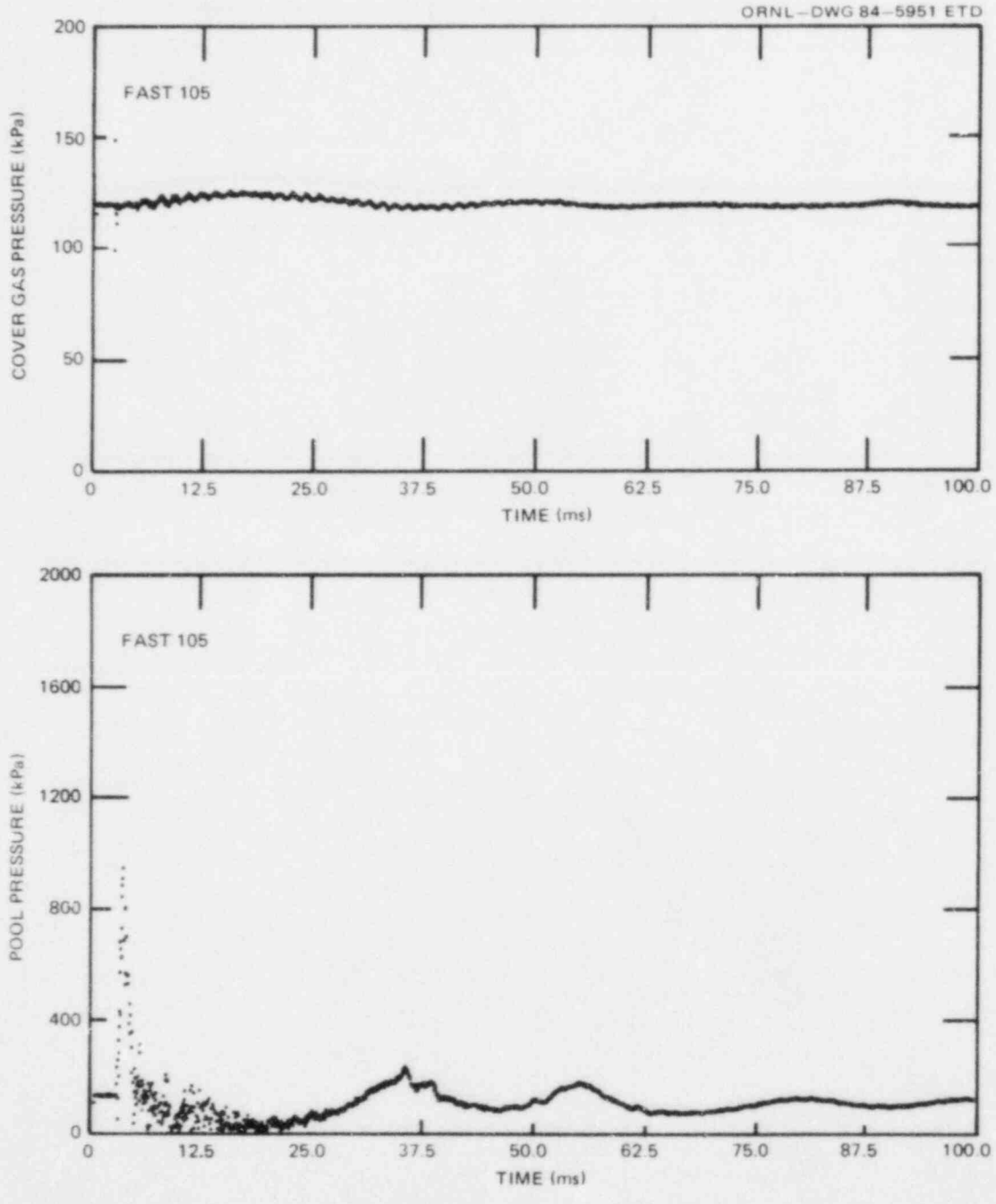

Fig. 8. Measured pressures, FAST-105 (baseline cover gas pressure is 120 kPa).

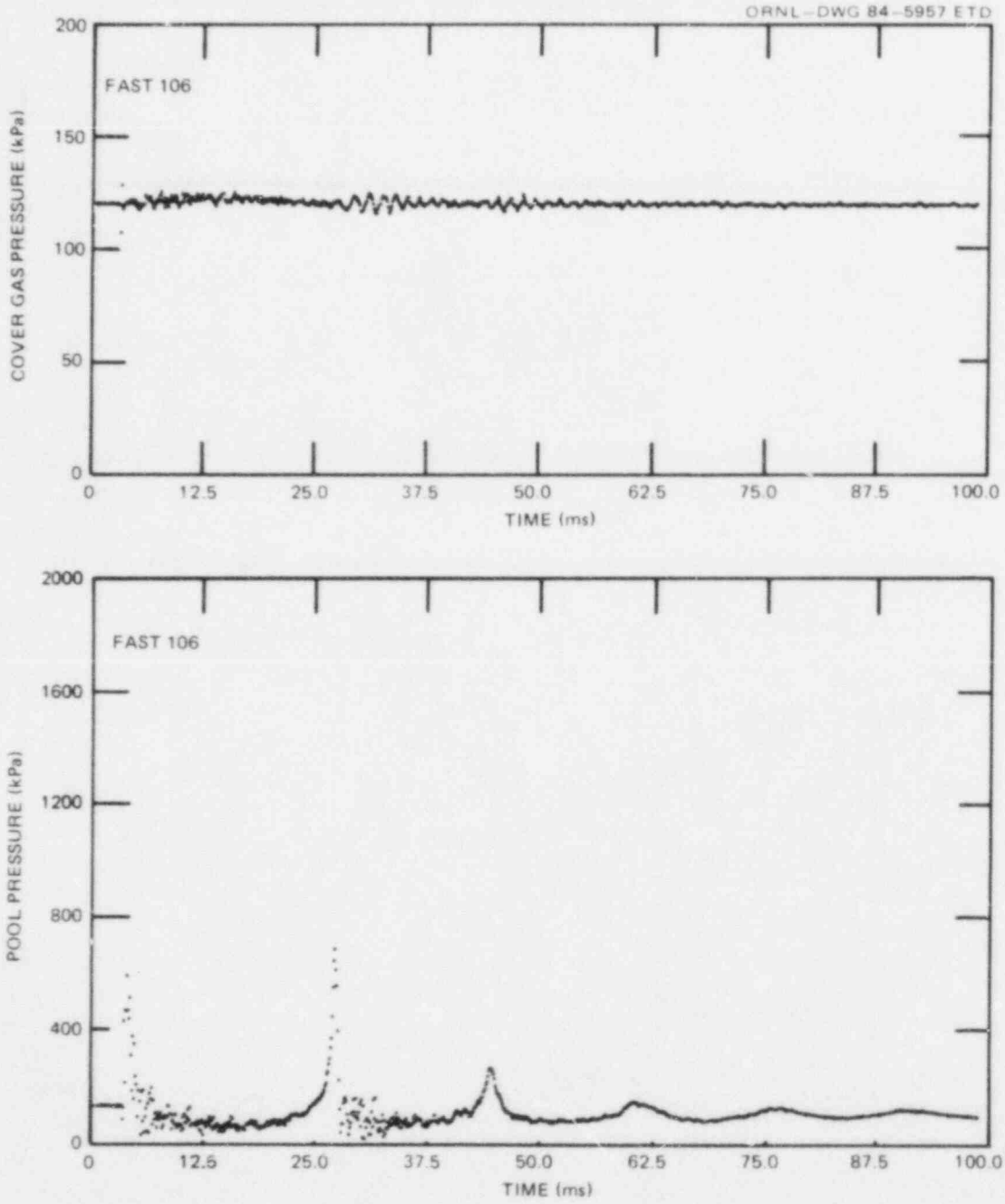

Fig. 9. Measured pressures, FAST-106 (baseline cover gas pressure is 120 kPa).

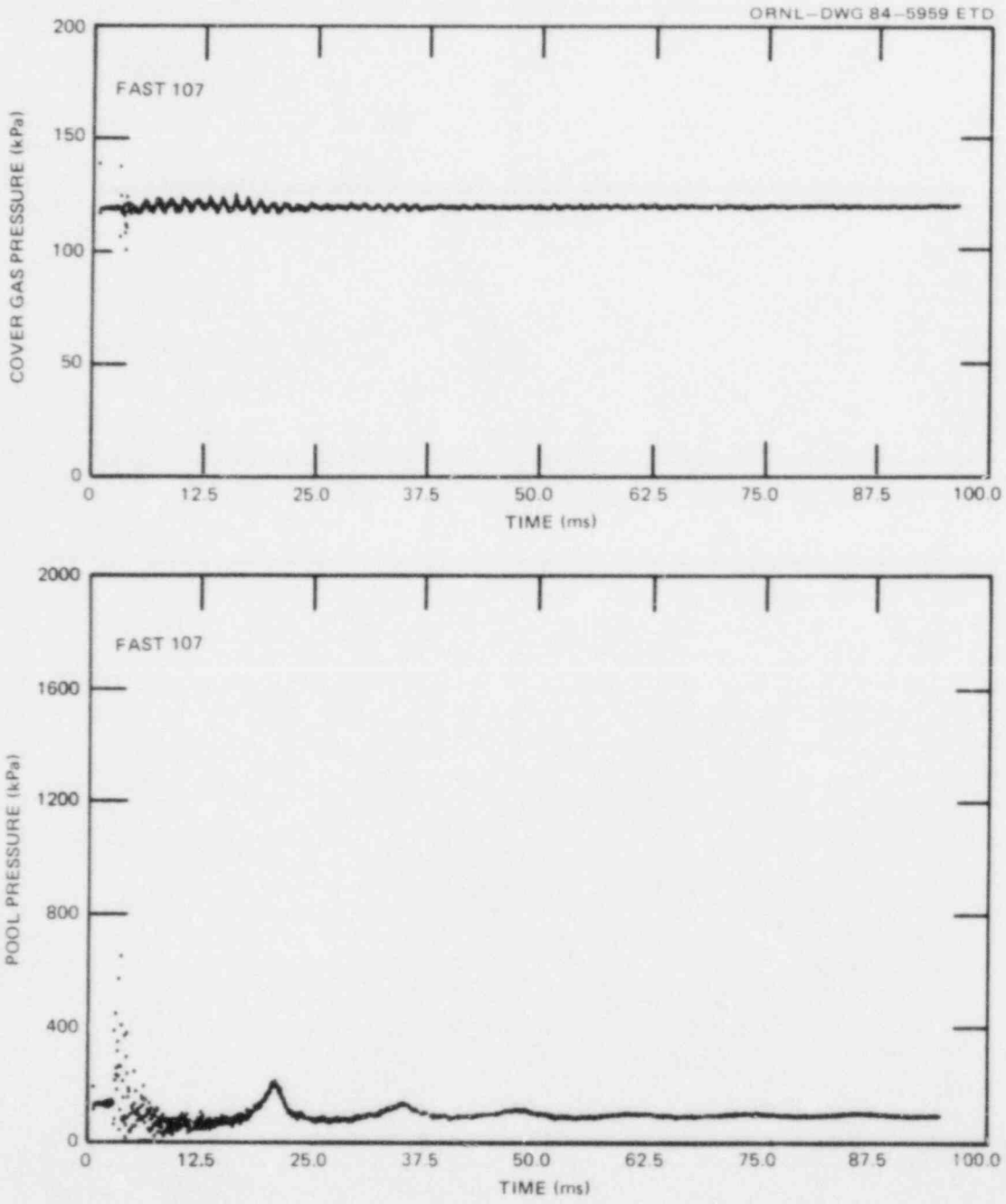

Fig. 10. Measured pressures, FAST-107 (baseline cover gas pressure is 121 kPa).

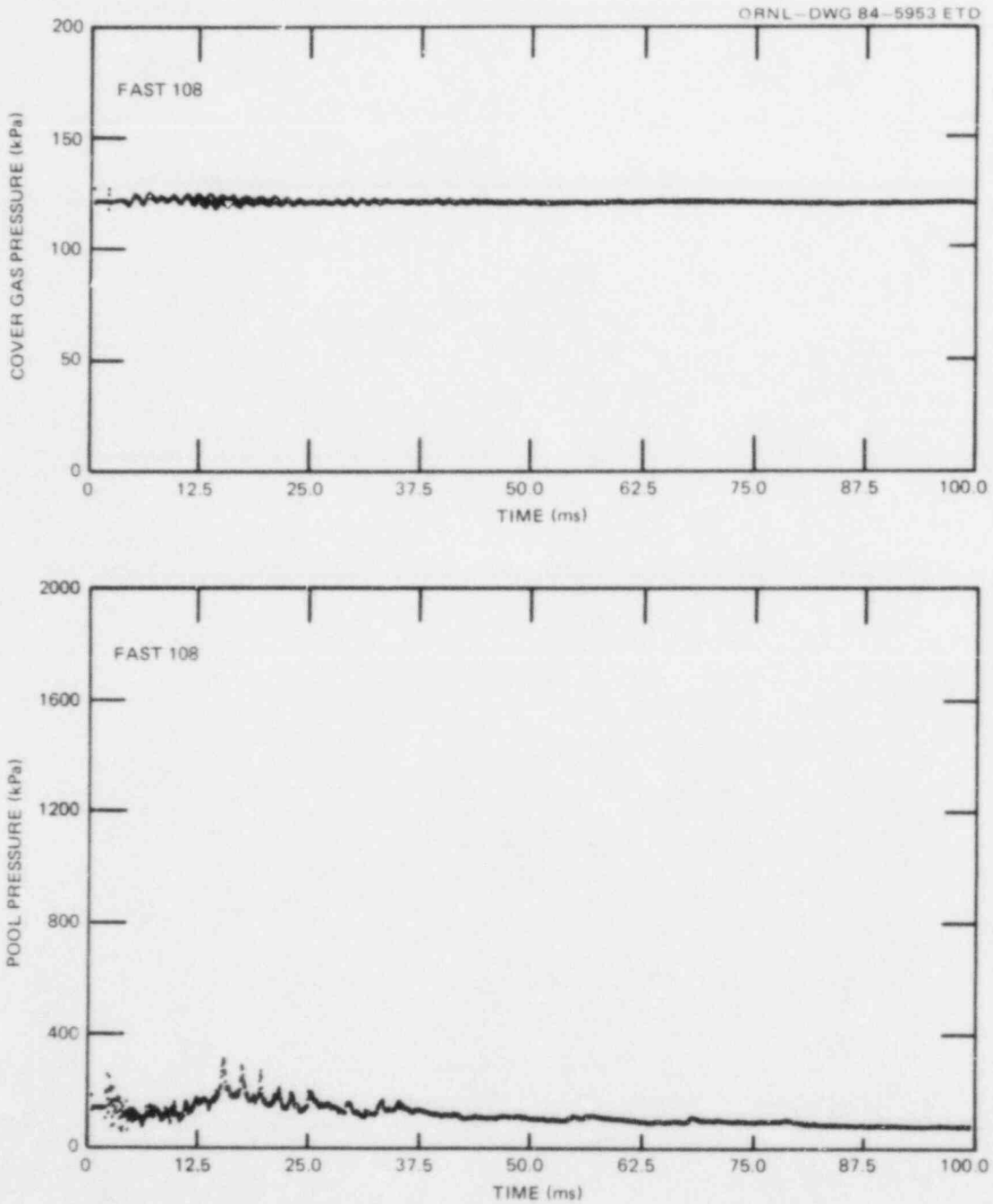

Fig. 11. Measured pressures, FAST-108 (baseline cover gas pressure is 120 kPa).

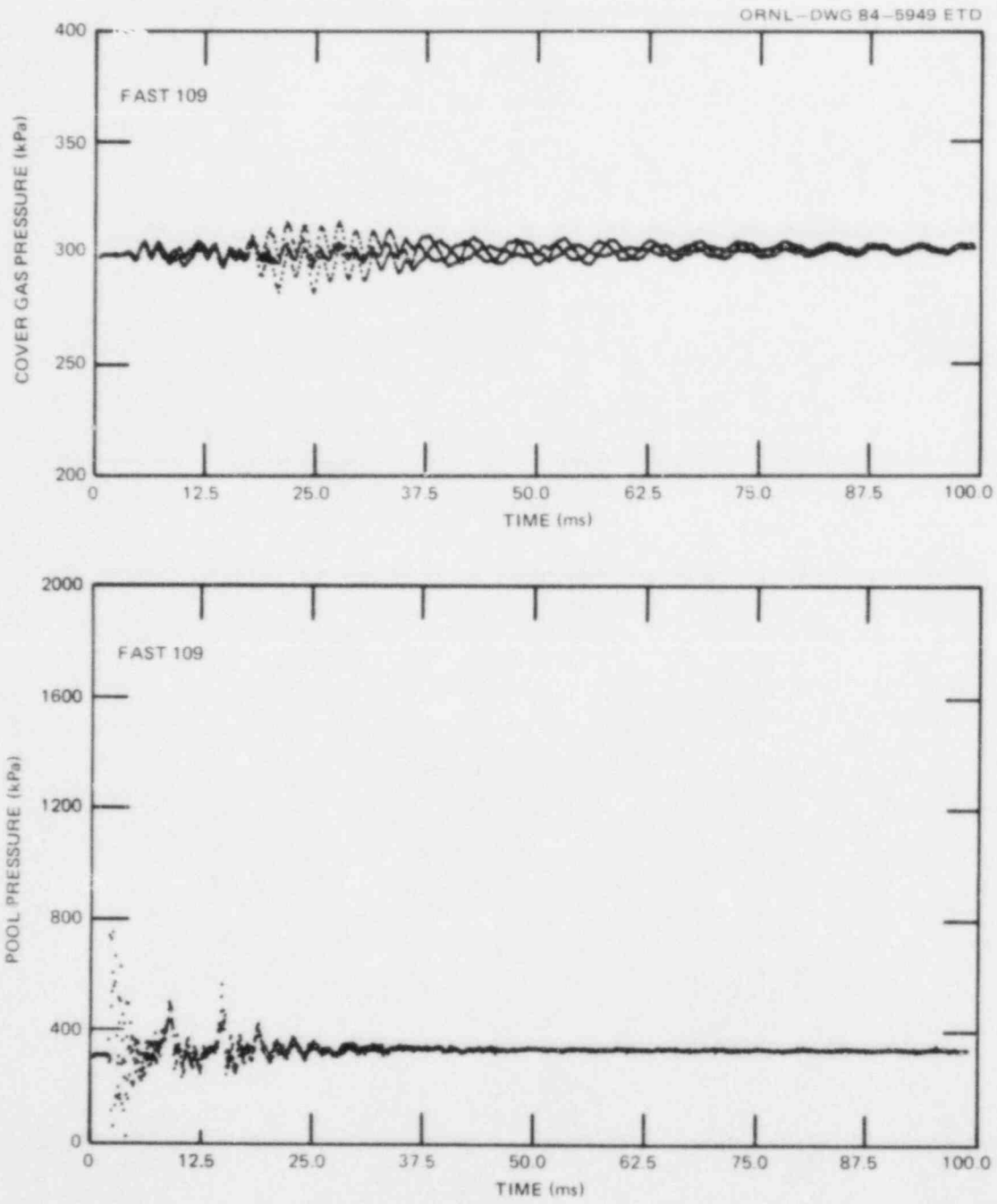

Fig. 12. Measured pressures, FAST-109 (baseline cover gas pressure is 300 kPa).

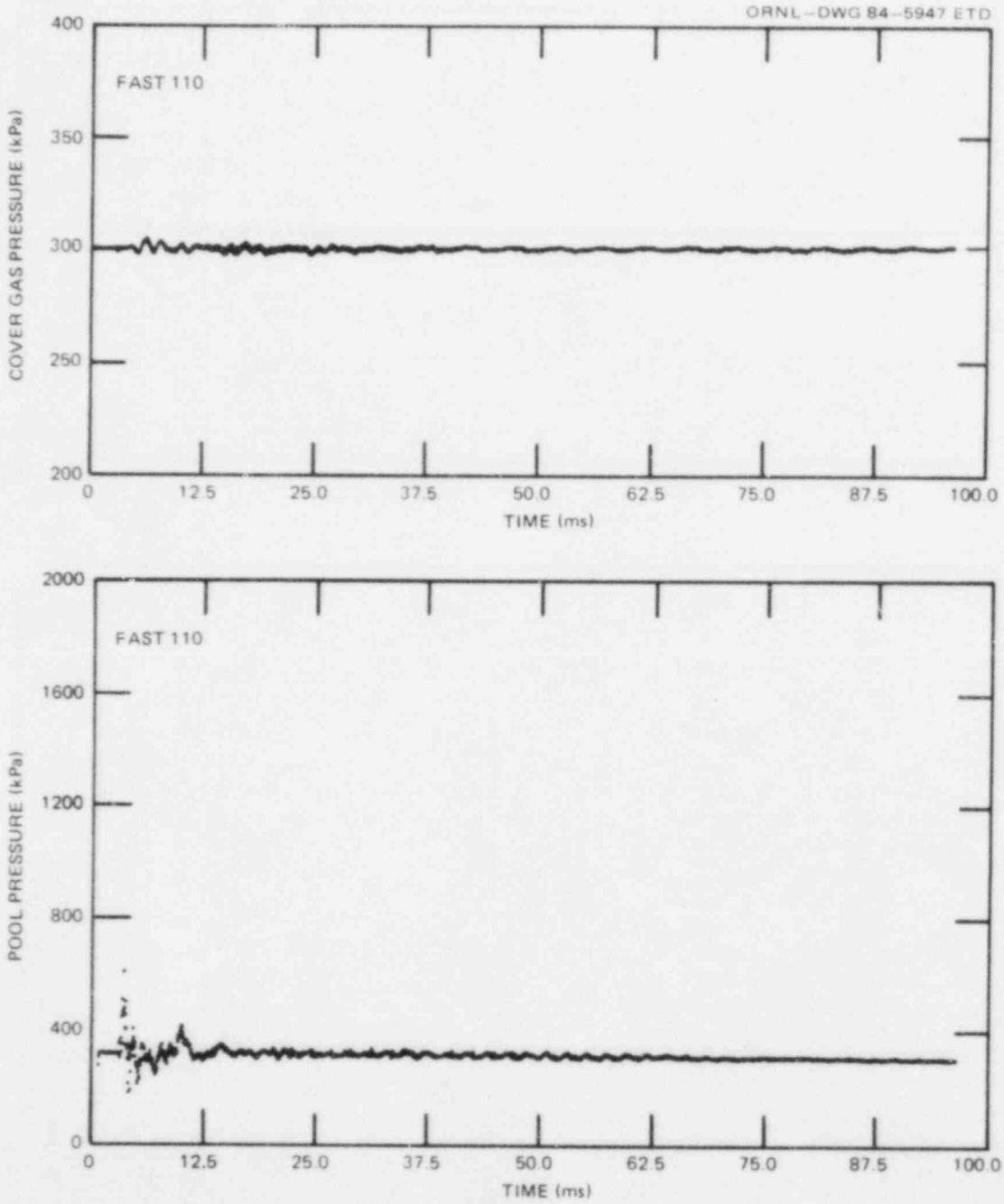

Fig. 13. Measured pressures, FAST-110 (baseline cover gas pressure is 300 kPa).

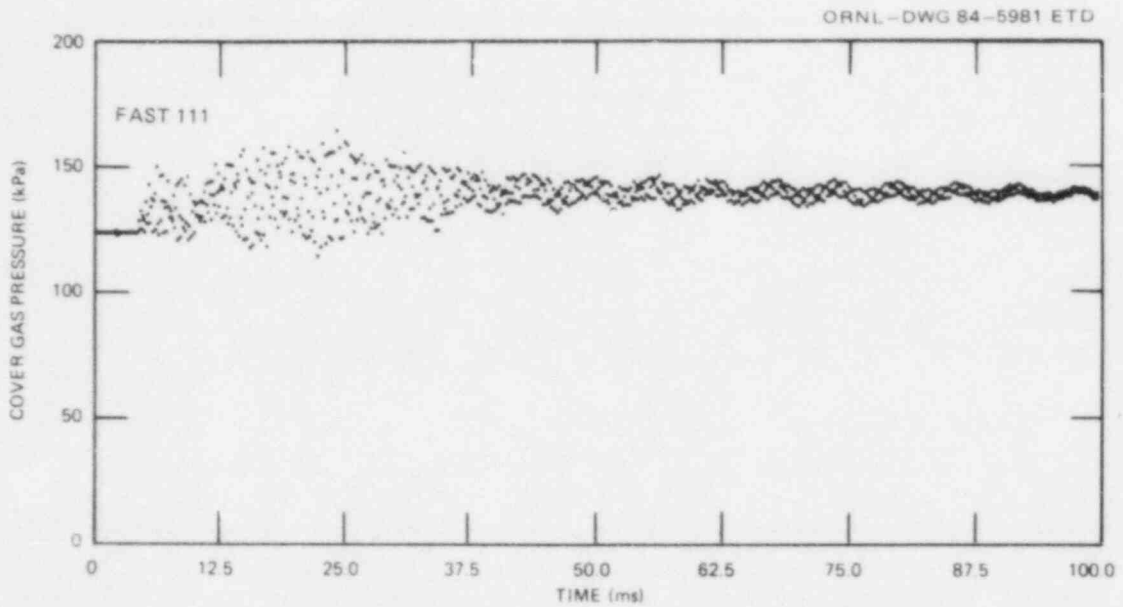

Fig. 14. Measured pressure, FAST-111 (baseline cover gas pressure is 122 kPa).

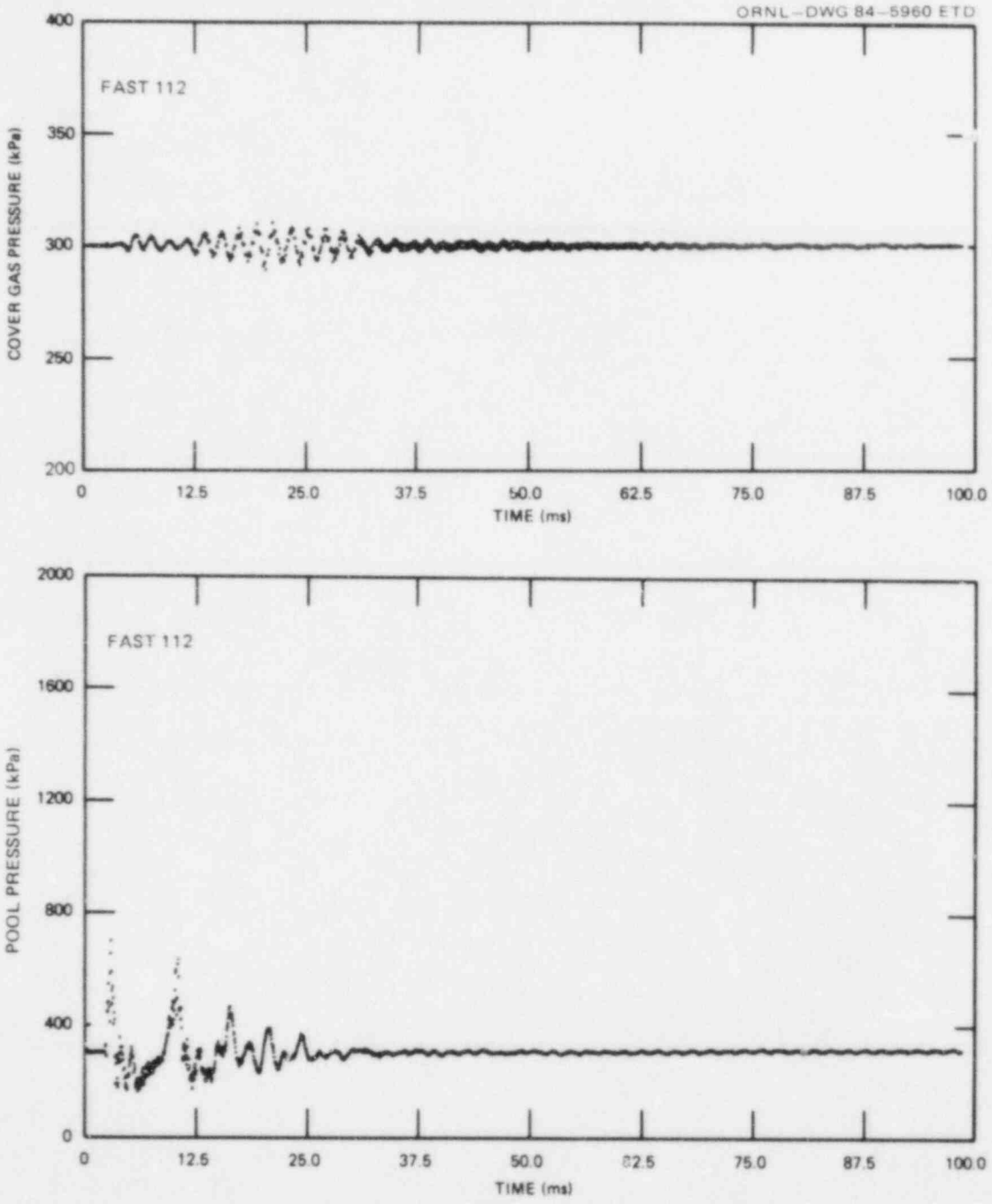

Fig. 15. Measured pressures, FAST-112 (baseline cover gas pressure is 300 kPa).

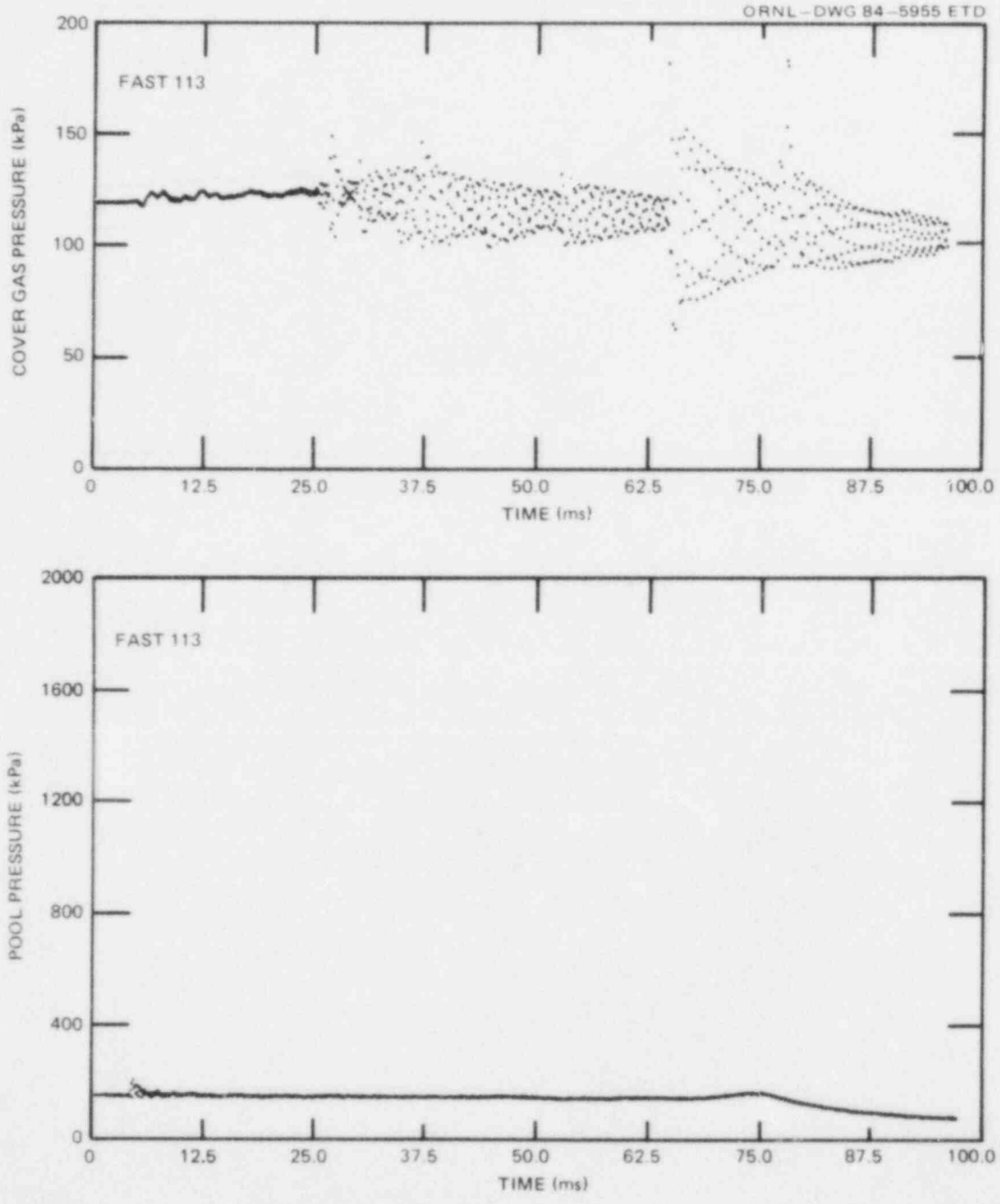

Fig. 16. Measured pressures, FAST-113 (baseline cover gas pressure is 119 kPa).

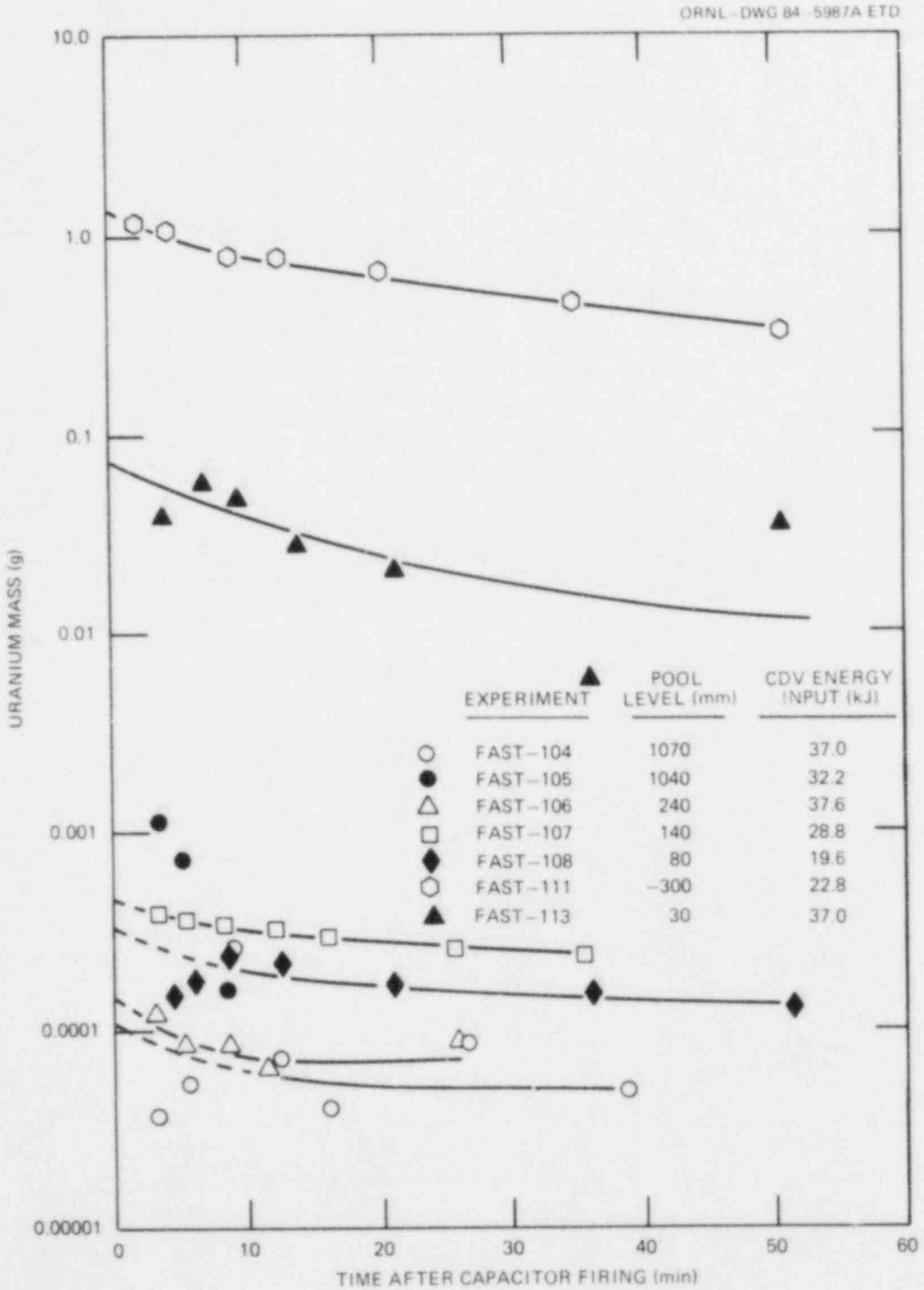

Fig. 17. Measured uranium mass in ~120 kPa argon cover gas (curves fitted visually).

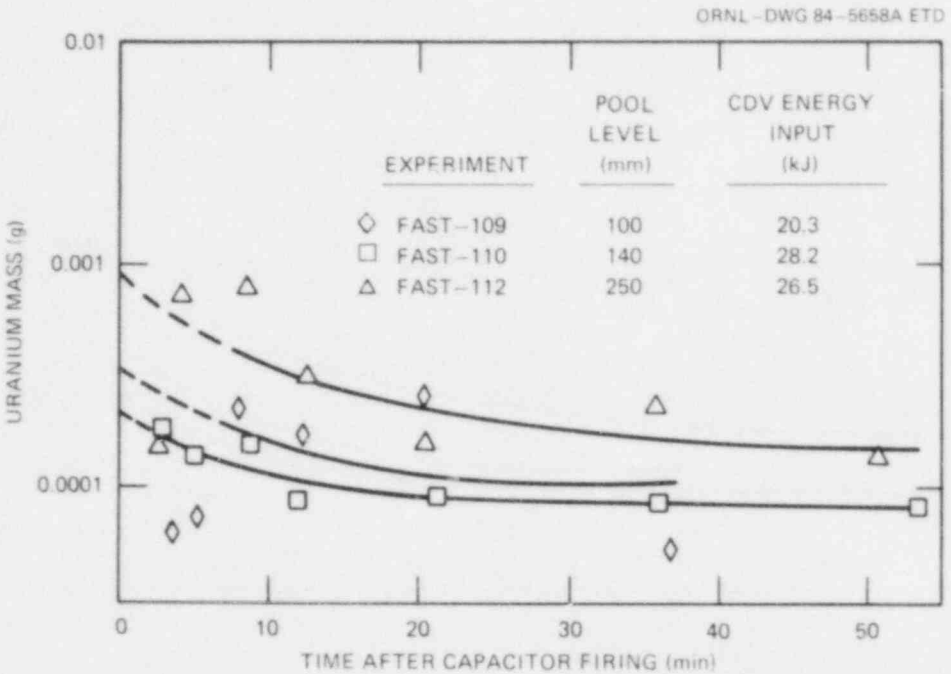

Fig. 18. Measured uranium mass in ~300 kPa argon cover gas (curves fitted visually).

4. ANALYSIS OF EXPERIMENTAL DATA

4.1 Pressure Data

Pressure data presented in Sect. 3 are analyzed in this section. Cover gas pressure data are used to calculate an estimate of the maximum, multiphase, bubble size. Pool pressure data are analyzed with the aid of theoretical bubble and pool dynamics models to examine the role and nature of shock waves and dynamic pressures in FAST undersodium experiments. A correspondence between pool pressure and bubble pressure is suggested that accounts for the inertia of the pool. Results of computational simulations, which support the idea that sodium flow is more dynamic at low pool levels, are also discussed.

4.1.1 Cover gas pressure and calculated bubble size

An estimate of the submerged, multiphase, bubble size was made by calculating the volumetric compression of the cover gas. Assuming liquid sodium incompressibility, the bubble underwent a simultaneous volumetric expansion of magnitude equal to the cover gas compression. Visual comparison of the pool and cover gas pressure traces identified an inverse correlation. For example, pressures measured from 0 to ≈40 ms in FAST-104 were inversely correlated (see Fig. 19); the cover gas pressure was highest when the pool pressure was lowest and vice versa. Also, the lower cyclic frequencies evident in these segments of the pressure traces were clearly similar (≈25 Hz), suggesting a strong coupling between pool and cover gas pressures during the early phase of the bubble pulsation. High-frequency components (300 Hz or greater) of the cover gas pressure traces were viewed as anomalous signals because they could not be correlated to any observable feature of the pool pressure traces. This suggested that the lower frequency components were indicative of pulsatile bubble behavior. On this basis, bubble pulsation frequencies varied from ~20 to 50 Hz in the FAST undersodium experiments.

Bubble sizes were estimated using cover gas pressure data in conjunction with the appropriate constitutive equation for the gas. Isentropic approximations were valid at these frequencies (20 to 50 Hz) with specific heat ratio for argon given by $\kappa = 1.67$. Bubble size measurements were standardized by calculating the radius of an equivalent spherical volume:

$$R = \left(\frac{3}{4\pi}\left\{V_{B_o} + V_{CG_o}\left[1 - (P_o/P)^{1/\kappa}_{CG}\right]\right\}\right)^{1/3} . \qquad (1)$$

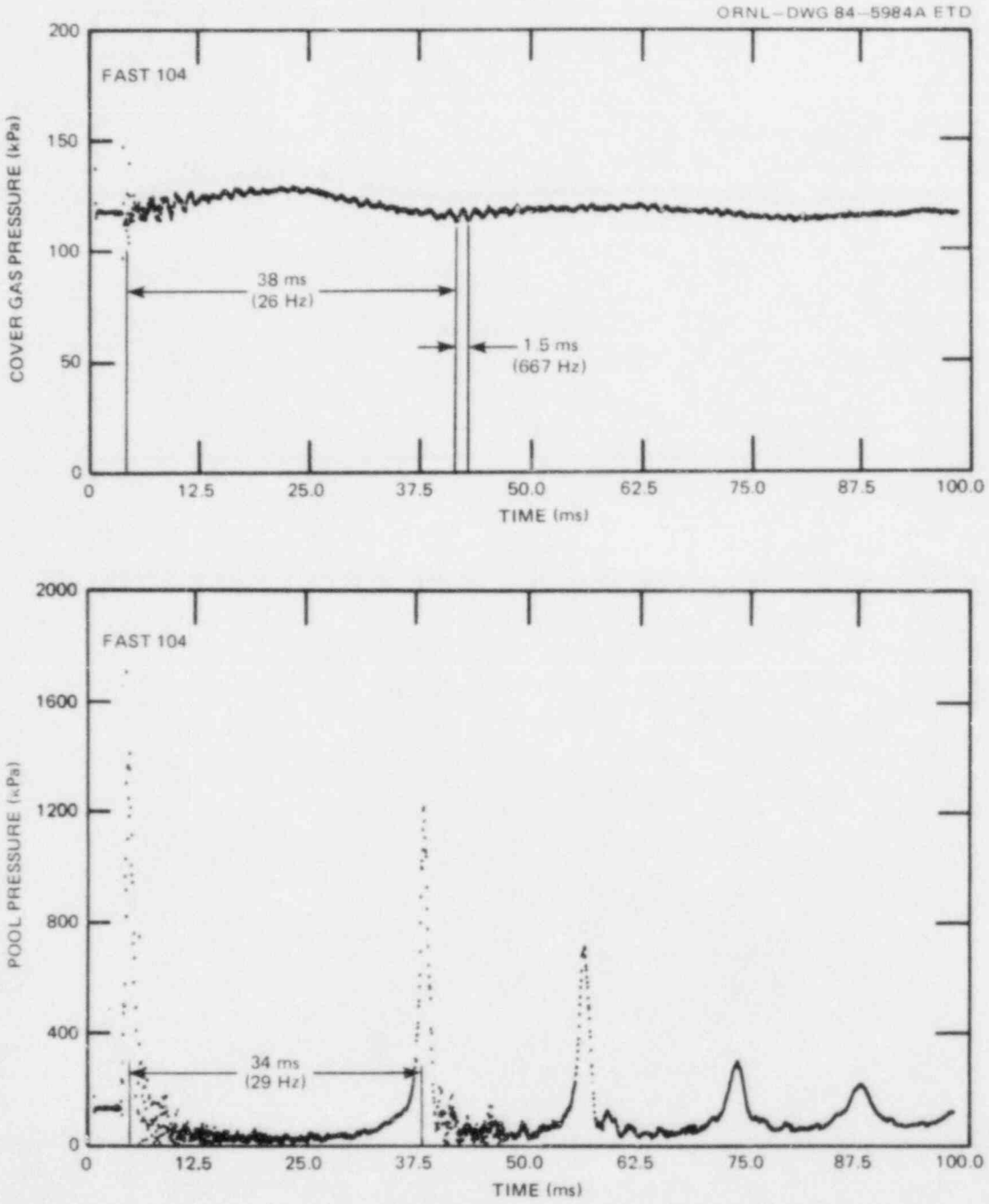

Fig. 19. Frequency characteristics of cover gas and pool pressure traces (FAST-104).

An initial bubble volume of ~15,000 mm^3 was chosen,* assuming that the mixture initially occupied intra-assembly gaps in the vaporizer between microspheres and between the quartz and steel tube. Calculations of the maximum radius of the bubble were made using peak cover gas pressure measurements (neglecting the high-frequency components) for every under-sodium experiment; results are listed in Table 5. Also shown are bubble radii calculated by Webb[15] using the UVABUBL-II computer simulation of pool and bubble dynamics.† Webb's results were more direct because they were based on bubble kinematics and dynamics instead of cover gas pressures. Still, agreement between the empirical and theoretical values was good, suggesting an underlying consistency in the models.

*A precise estimate of this number was not needed because Eq. (1) was relatively insensitive to it.

†See Appendix for a description of UVABUBL-II.

Table 5. Comparison of calculated maximum bubble radius using experimental measurements and UVABUBL-II predictions

Experiment No.	R_{MAX} (mm)	
	Equation 1	UVABUBL-II[a]
FAST-104	100	98 ± 8[b]
FAST-105	80	98 ± 8[b]
FAST-106	110	100 ± 7[c]
FAST-107	100	99 ± 8[c]
FAST-108	80	
FAST-109	90	
FAST-110	60	63
FAST-112	60	63
FAST-113	130	

[a]Uncertainties represent ±1σ of the average maximum equivalent-sphere radius.

[b]Statistical averages obtained from 15 UVABUBL-II runs.

[c]Statistical averages obtained from two UVABUBL-II runs.

4.1.2 Pool pressure

Pool pressures differed from cover gas pressures because hydrostatic, hydrodynamic, and shock wave effects were more pronounced in the pool.* These differences were attributed to (1) the greater inertia of the pool compared to the cover gas and (2) the proximity of the pool pressure transducer to the pulsating bubble.

4.1.2.1 Shock wave effects. Underwater chemical and nuclear explosions have been studied extensively[16,17] to determine the pressures generated from resulting shock waves and bubble pulsations. Models developed in those studies were applied to the analysis of vapor dynamics in the FAST experiments. Characteristically, energy partitioning between the bubble pressure and the primary shock wave is 47|53% for chemical explosions[16] and 40|60% for nuclear explosions.[17] Based on this data and the observed pressure spikes in the pool pressure records, the existence of shock waves in FAST experiments could not be precluded. The aim of this section is to examine those conditions under which shock waves could be generated and to determine whether shock waves could be identified in the pool pressure record.

Shock waves are generated in continuous media when the rate at which pressure is applied exceeds the rate at which the resulting disturbance can be propagated [e.g., see Shapiro[18] (shock waves in fluids) or for a general discussion, Whitham[19]]. "Small" disturbances propagate at the speed of sound of the medium; the propagation speed for larger disturbances has a more complicated dependence on properties of material and state (see Cole[16]). To a first approximation in the FAST experiments, the propagation speed of disturbances in the pool was taken as the speed of sound in sodium at 810 K: ~2300 m/s.

The multiphase mixture of UO_2 and xenon contained in the vaporizer assembly was both a pressure source and a mass source of varying intensities. As the steel tube ruptured, the vapor-gas mixture was expelled explosively into the sodium pool forming a dynamic multiphase bubble. Although expulsion could occur very rapidly, it would not occur instantaneously because of the inertia of both the mixture and the pool and because the initiating pressure disturbance had a finite propagation speed. The disturbance, or shock, was roughly equal to the pressure "discontinuity" between the mixture and the pool. The shock was probably quite intense because rupture could not occur unless the mixture pressure exceeded the dynamic rupture pressure of the quartz and steel tubes. It appears, therefore, that the shock intensity depended on the extent of vaporization during discharge and the rupture characteristics of the quartz and steel tubes. Historically, these factors have been associated with CDV energy input.

Calculations were made that related CDV energy input to the Mach number M at the bubble interface to determine whether the spikes in the pool pressure record represented shock waves. These estimates were based on the hydrodynamic theory of compressible flow (e.g., Ref. 18). If $M^2 \ll 1$, a flow is said to be "incompressible" because the propagation speed of flow-related disturbances is much greater than the flow speed so

*The hydrostatic pressure of the sodium pool was relatively small (i.e., <9 kPa).

that, from the standpoint of an observer moving with the flow, disturbances propagate instantaneously. Under these conditions, pressure waves cannot overtake one another, and shock development does not occur. These concepts were used to interpret the early phase of the pool pressure traces where shock effects would be more likely found.

The total mechanical energy of an expanding, submerged bubble was related to the Mach number at the bubble interface using Pritchett's model.[17] To apply this model to the analysis of FAST-type vapor bubbles, a method of estimating mechanical energy was postulated. Recall that the calculated temperature distribution in the sample at the end of high preheat showed that the sample was partially molten (Fig. 3). This suggested that vaporization began during capacitor discharge and that the CDV energy input was proportional to the mechanical energy of the expanding bubble. During the early phase of bubble growth, potential energy was neglected compared with the kinetic energy of the pool because gravitational effects are negligible when the bubble is small. The expression for Mach number is simplified considerably in this case:

$$M = \frac{1}{C}\left(\frac{E_o}{2\pi\rho}\right)^{1/5} t^{-3/5} \quad . \qquad (2)^*$$

Using this equation to calculate the Mach number at t = 0.002 s (corresponding to the earliest spikes in the pressure records) with characteristic FAST experimental parameters E_o = 30 kJ, C = 2296 m/s, and ρ = 820 kg/m^3, showed that

$$M = 0.026 \quad , \qquad (3)$$

and

$$M^2 = 0.00066 \ll 1 \quad . \qquad (4)$$

This estimate indicates that the incompressible approximation is valid and that the spikes in the pool pressure records did not represent shock waves.

Also note that the equipment used to measure pressure was not designed for shock wave applications. The dynamic frequency response of the pressure sensor electronics was too low to allow for accurate processing of a shock wave signal. The following example demonstrates this point. The thickness of a shock wave is typically ~10^{-2} μm.[16] If the shock wave propagates at or near the acoustic speed in sodium (i.e.,

---

*In the original report,[17] the bracketed denominator appeared as 25ρ. We have been unable to duplicate Pritchett's result and believe that this term should be 2$\pi\rho$ instead. Equation (2) is modified accordingly.

2296 m/s at 810 K), the effective frequency of the wave is ~230 GHz. The rated cutoff frequency of the pressure sensor electronics is only ~10 KHz. This mismatch means that a shock wave signal would be "filtered" by the electronics or "conditioned" into some other waveform.

4.1.2.2 Hydrodynamic effects. The pressure differential between the bubble and the pool consists of hydrodynamic components that could initiate fluid flow within the pool. One of these components is the dynamic, or flow-induced, pressure:

$$P_D = \rho \frac{q^2}{2} . \tag{5}$$

A formula for estimating dynamic pressures, assuming spherical-source potential flow with bubble interface velocities based on a bubble-size to pulsation-time ratio, is

$$P_D = \frac{1}{2} \rho \left(\frac{\partial \phi}{\partial r}\right)^2 , \tag{6a}$$

where

$$\frac{\partial \phi}{\partial r} = q_B \, (R/r)^2 , \tag{6b}$$

and

$$q_B = R/t . \tag{6c}$$

A typical value of P_D calculated at r = 230 mm (corresponding to the radial position of the pool pressure transducer), using $R = R_{MAX}$ = 100 mm and t = 10 ms, is 1.46 kPa. For these conditions, dynamic pressures clearly made a negligible contribution to the measured pool pressures.* Computer simulations[15] predicted close agreement between pool and bubble pressures in high pool-level experiments. This further suggests that the dynamic pressure was negligible and that the measured pool pressure closely approximated the instantaneous (i.e., static-plus-impulse) pressure:

$$P = P_s + \rho \frac{\partial \phi}{\partial t} . \tag{7}$$

---

*The efficacy of spherical bubble approximations is limited to high pool-level experiments (FAST-103–105). Bubble shape distortions occur in the proximity of a free surface.[20-22]

In low pool-level simulations, significant discrepancies were noted[15] between bubble and pool pressures throughout virtually the entire simulation with peak pool pressures an order of magnitude lower than peak bubble pressures. These discrepancies were probably real, suggesting a more dynamic sodium flow in low pool-level experiments (FAST-106–110, -112–113) caused by the relatively lower inertia of the pool. For example, a reduction in peak pool pressures was observed when FAST-106 and -107 data were compared with FAST-104 and -105, respectively; results were consistent with the theoretical predictions.*

It appears, therefore, that pool pressure measurements in the low pool-level experiments were not indicative of bubble pressure. Pronounced pressure differences, related to flow-induced pressure reductions in the pool, were probably larger in low pool-level experiments because of lower pool inertia in those experiments. In high pool-level experiments, pool pressure measurements more closely tracked bubble pressures. Other differences were probably caused by spatial variations of impulse pressure.

4.2 Aerosol Data

Based on aerosol data presented in Figs. 17 and 18, release to the cover gas was extremely low (i.e., $\lesssim$1 mg or $\lesssim$0.006% of pellet stack mass) in every experiment except FAST-111 and FAST-113. Significantly higher release was noted in these two experiments. In FAST-111, disassembly occurred within the cover gas volume rather than in the pool, so attenuating effects of the pool were insignificant. Release was relatively abundant ($\approx$1.5 or $\approx$9% of pellet stack mass) as expected, demonstrating that (1) measurement procedures were satisfactory, (2) measurements of low release in previous experiments were probably accurate, and (3) release was strongly impeded by the layer of sodium between the vaporizer and the pool surface.

The release-vs-depth dependence was complicated by free surface effects that became increasingly pronounced at shallow depths. For example, the 100-fold increase in release from the pool in FAST-113 may have been illusory because visual inspection and chemical analysis of aerosol samples showed probable contamination by pool material that might have contributed to the UO_2 content. Much larger than normal quantities of sodium (~50 fold) were measured; UO_2 debris suspended in the sodium, probably deposited on the filters following the near-surface vapor explosion. Data supporting this conjecture will be presented in Sect. 4.2.3.

The remainder of this section deals with the relatively low aerosol release in undersodium experiments (FAST-104–110, -112, -113) of which all except FAST-113 were typical examples. An indicator of aerosol release based on a bubble-size to pool-level ratio is proposed and is shown to be consistent with experimental observations. Hydrodynamic effects are also analyzed. Particular studies show that aerosol release could be strongly impeded by pool surface effects.

---

*Energy input in these comparisons was nearly equal.

4.2.1 Bubble size and aerosol release

Although the release of aerosol particles to the cover gas can be motivated by other factors, the phenomenological approach adopted here assumes that the aerosol was contained in the bubble and that bubble motions dictated aerosol transport within the pool because (1) bubble and aerosol originated from the same source and (2) bubble pressures could generate fluid motions within the pool. The last point implies that buoyant migration was negligible over the time scale of several bubble pulsations. Significant buoyant migrations were unlikely because the measured pulsation frequency was ~50 Hz, too high for buoyancy to be effective.

Assuming that this phenomenology adequately describes events, aerosol release can be determined by analyzing bubble motions. To simplify the analysis of these complex motions, only the first radial pulsation of an equivalent spherical volume was considered. Pressure measurements indicated that succeeding pulsations were weaker; the first volumetric expansion was the biggest. The spherical volume approximation becomes increasingly accurate for bubble pulsations in high pool-level experiments because the free surface does not disturb bubbles at great depth.[21] For these conditions, contained aerosol particles traveled no further than a bubble maxima (i.e., maximum bubble radii) during any pulsation with the extent limited by the first pulsation. If this distance did not exceed the vertical distance between vaporizer and undisturbed pool surface and if the pool surface above the bubble did not deflect downward, the bubble would not break the surface, and aerosol release would not occur. These concepts are embodied in an aerosol release parameter $\gamma \equiv h/R_{MAX}$ whose definition implies

$\gamma < 1$ when the bubble breaks the surface (i.e., aerosol release occurs),

and (8)

$\gamma > 1$ when the bubble does not break the surface (i.e., aerosol release does not occur).

Note that γ is not an absolute indicator of aerosol release because situations can be envisioned for which these criteria do not apply. For example, $\gamma < 1$ does not ensure that release occurred unless drainage of the sodium layer above the bubble was completed during the first expansion. Also, some aerosol may be transported to the cover gas by noncondensible, xenon bubbles. Nevertheless, γ helps visualize the kinematics of release and will be used later to characterize bubble and aerosol behavior using more sophisticated models.

Virtually all of the aerosol data presented in Figs. 17 and 18 are consistent with the model just discussed. Aerosol release was extremely low in every undersodium experiment except FAST-113 because the maximum transit distance of a particle was less than the vertical distance between vaporizer and pool surface; that is, $\gamma > 1$. This conclusion is

based on data in Figs. 20 and 21 where pool level and maximum bubble radii are displayed on the same scale. It appears that a strictly pulsating spherical bubble could not break the pool surface in any experiment except perhaps FAST-113 where the pool level was too low to confine a 130-mm bubble. As mentioned earlier, a significantly higher release was measured in FAST-113.

In very low pool experiments (FAST-108, -109, and -113), surface interactions were strong enough to invalidate simplified bubble and pool approximations and make the aerosol release criteria doubtful. The proximity of the surfaces resulted in a highly dynamic interaction that affected bubble and pool surface shape and bubble position. The interaction was associated with higher dynamic pool pressures P_D and was confirmed by measurements (see Sect. 4.1.2.2) and computer simulations.[15] It remains to be shown how a more dynamic pool would be manifested, particularly with regard to surface shape, and how pool dynamics might influence aerosol release.

4.2.2 Free surface effects on aerosol release in low pool-level experiments

Several investigators[20-22] have shown that free boundaries influence the migration of pulsating bubbles. These results were used to interpret bubble motion and aerosol release in low pool-level experiments. Blake and Cerone[20] applied potential flow theory and the method of images to show that the direction of the bubble impulse (i.e., Kelvin impulse) depends on the type of boundary adjacent to the bubble. For free surfaces, the bubble impulse is directed away from the surface; a pulsating bubble migrates away from the surface. Using asymptotic expansions and more generalized free surface boundary conditions to account for the distortion of bubble and pool surface, Chahine[17] showed that a pulsation near a free surface generates a concave extension of the pool surface containing a "dome" or "finger" directly above the bubble. Collapse of the configuration generates a jet that is thought to repel the bubble downward. These effects, caused by the interaction between the bubble and pool surfaces, intensify as the pool level is lowered.

In the most comprehensive of these studies, Blake and Gibson[21] verified Chahine's findings using a more sophisticated hydrodynamic model and high-speed cinematography of vapor explosions in shallow water pools. The free surface effects were characterized by a single parameter $\gamma \equiv h_o/R_{MAX}$, previously used in this report to characterize release. Values of γ are compared between both studies in Table 6; kinematic similarity is suggested by numerical equivalence. Although equivalence was not exact, several of Blake and Gibson's cases approximated FAST experimental characteristics. These cases were used to qualitatively examine free surface effects on bubble and aerosol release in low pool-level experiments. Here, low pool-level experiments were those in which surface interactions were probable; that is, $\gamma < 2.2$. This condition is comparable to Chahine's limit criterion for undisturbed pool surfaces ($\gamma = 2.12$), determined by analysis and high-speed cinematography.

ORNL–DWG 84–5987B ETD

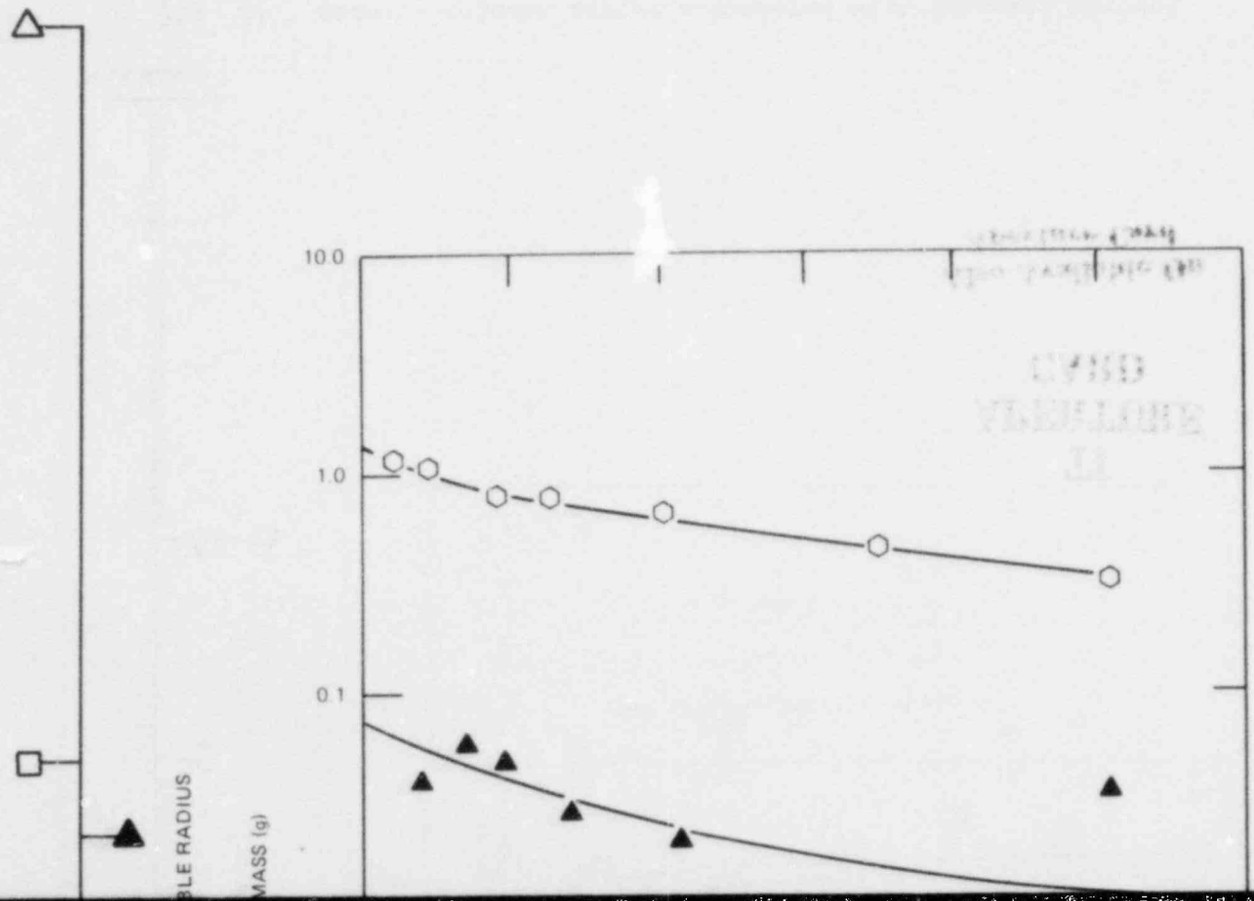

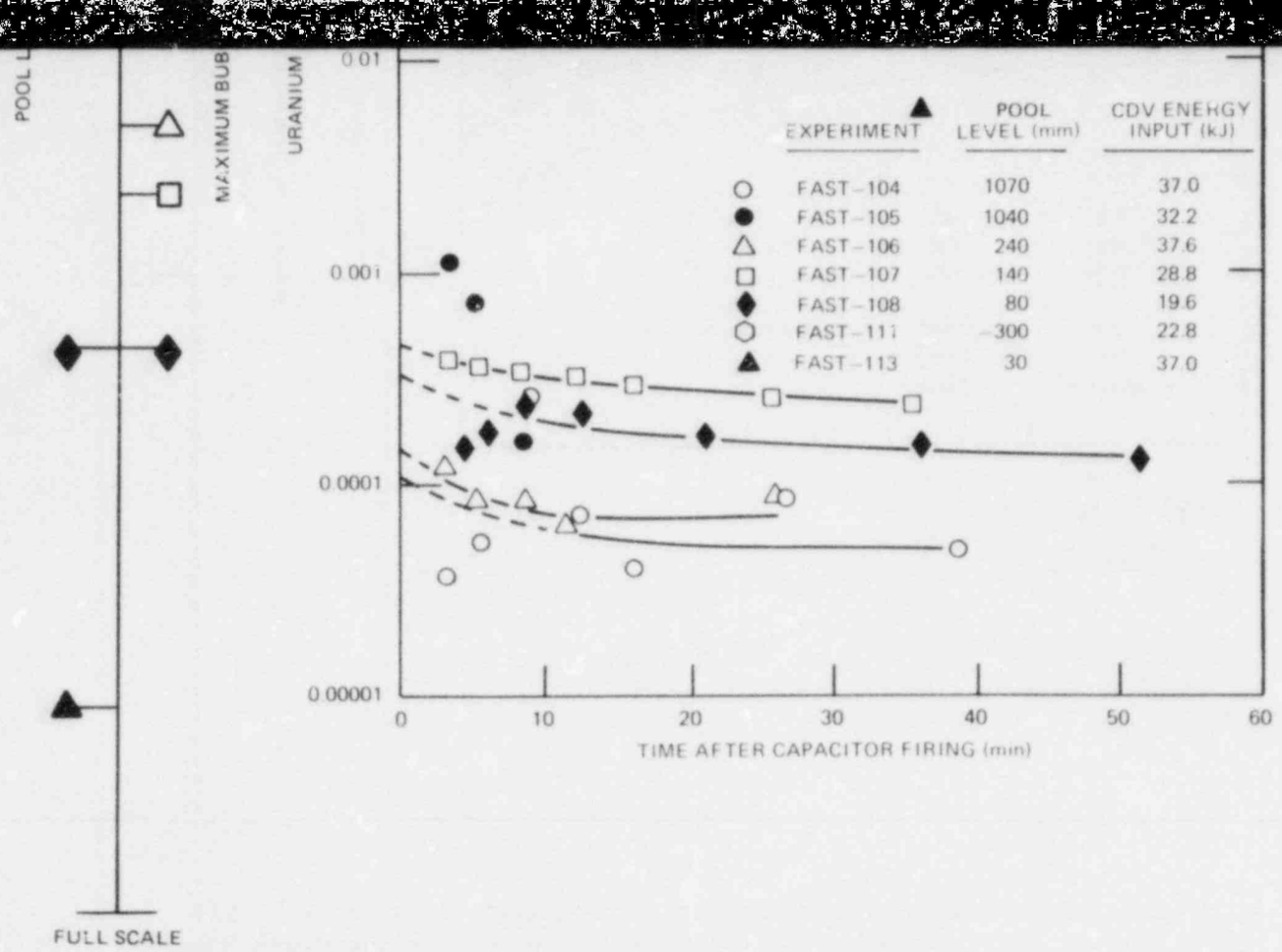

Fig. 20. Aerosol release criteria compared with measured aerosol released (low argon pressure ~120 kPa). Data indicate that aerosol release is small whenever $\gamma = H_o/R_{MAX} < 1$.

ORNL–DWG 84–5658B ETD

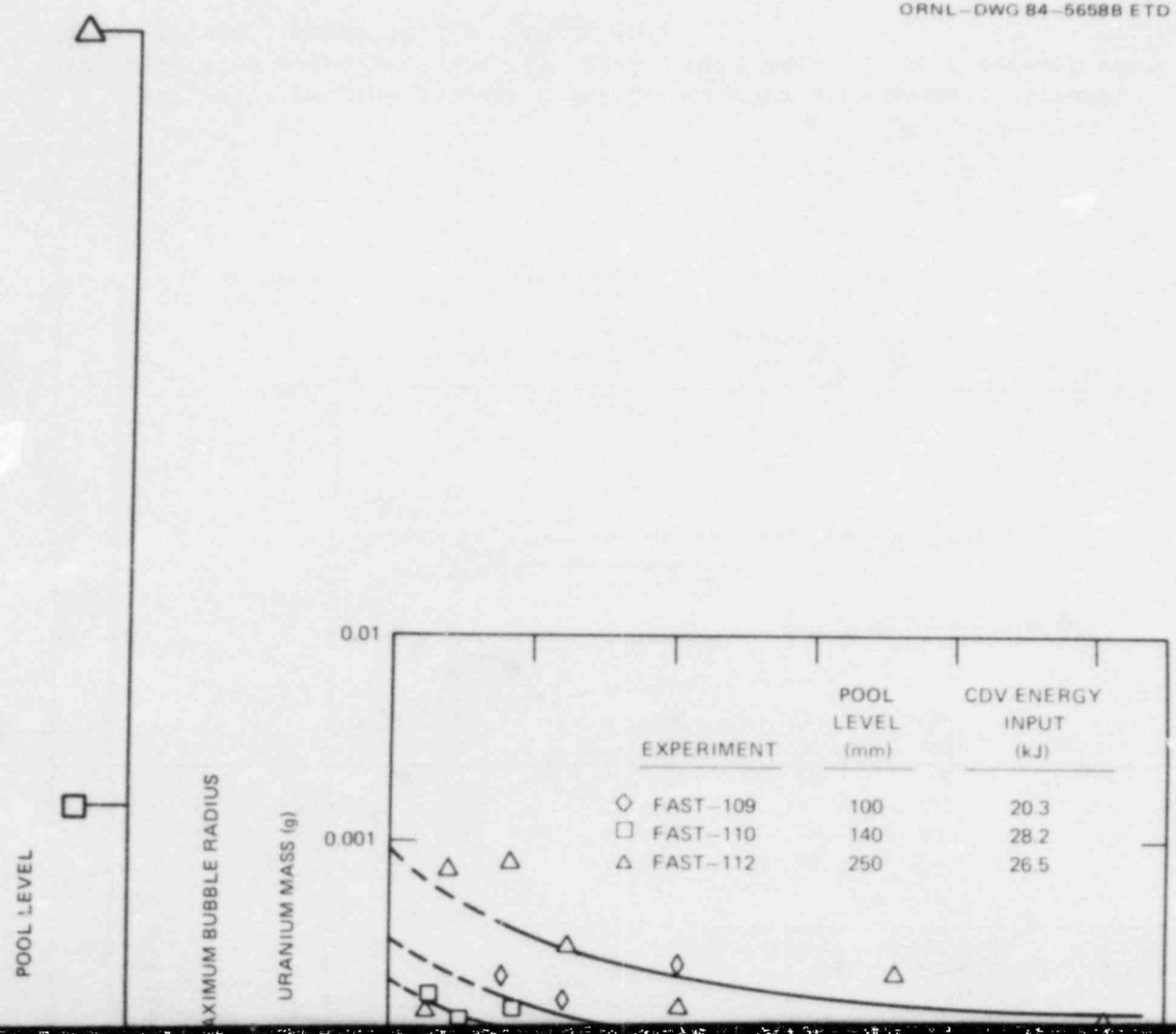

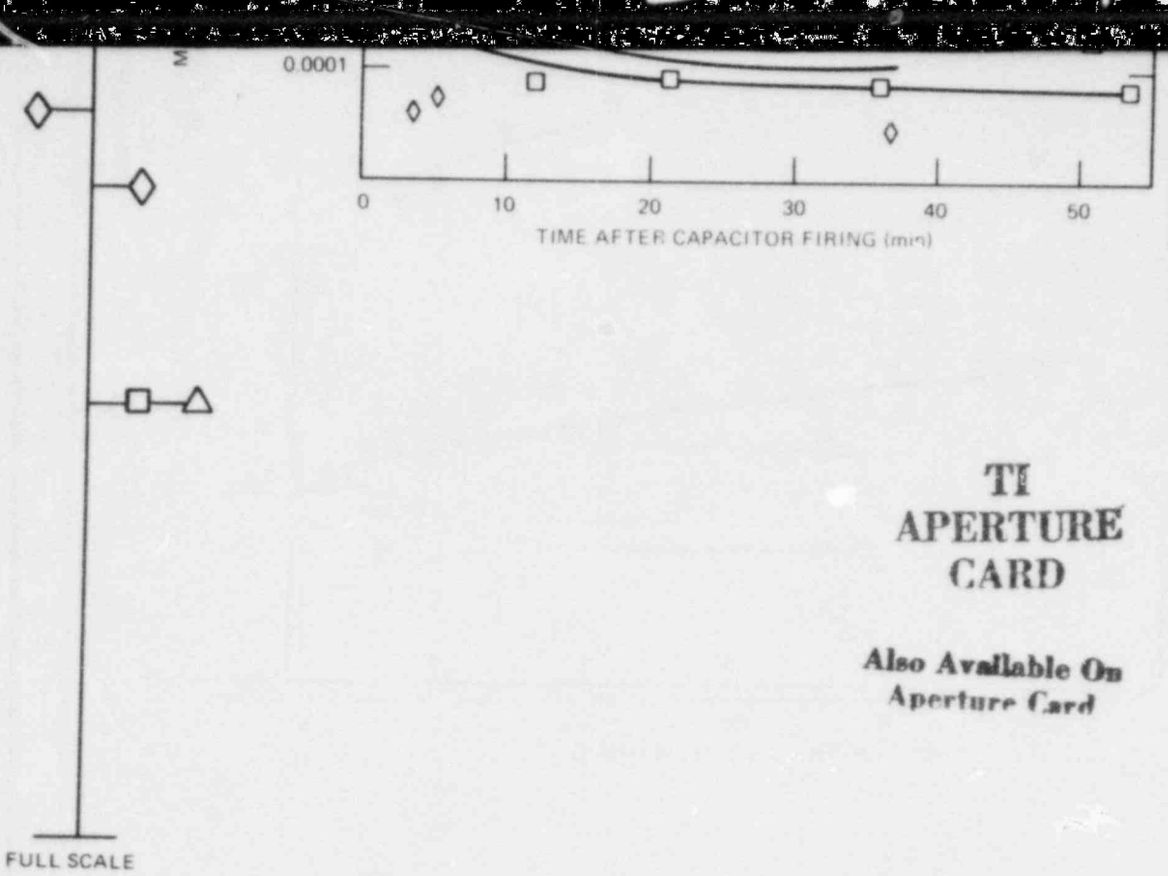

Fig. 21. Aerosol release criteria compared with measured aerosol released (high argon pressure ~300 kPa). Data indicate that aerosol release is small whenever $\gamma = h_o/R_{MAX} < 1$.

Table 6. Kinematic characterization of bubble pulsations ($\gamma = h_o/R_{MAX}$)

FAST undersodium experiments		Blake and Gibson[16]	
Experiment No.	γ	Case[a]	γ
FAST-104	10.6		
FAST-105	13.0		
FAST-106	2.2	A	1.68
FAST-107	1.4		
FAST-108	1.0	B	0.98
FAST-109	1.1		
FAST-110	2.3		
FAST-112	4.2		
FAST-113	0.2	C	0.56

[a]Designations assigned by the authors of this report.

Comparisons were divided into three categories:

Category I (FAST-106 and -107 and Case A)
Surface interaction is moderate; $1.2 < \gamma < 2.2$.

Category II (FAST-108 and -109 and Case B)
Surface interaction is strong; $0.8 < \gamma < 1.2$.

Category III (FAST-113 and Case C)
Surface interaction is very strong; $\gamma < 0.8$.

Bubble and pool surface profiles are presented in Figs. 22–25 for cases A–C. In every case, the bubble moved progressively away from the surface during collapse. Bubble displacement was greater during collapse, so the bubble center was farther from the pool surface at the end of the first cycle. The pool confined the bubble throughout the first oscillation even in cases where $\gamma < 1$. These confinements were provided by pool surface disturbances (domelike or fingerlike) located directly above the bubble. An exceptional example was case C where a finger extended several bubble maxima into the cover gas. Bubble surface instabilities of Rayleigh-Taylor type originated during the collapse phase; instabilities grew during collapse, as predicted by theory,[23] and could have caused bubble breakup into smaller volumes.

Applied to FAST experiments, these results suggested that the pool surface layer was extremely dynamic in very low pool-level experiments and that aerosol release was impeded by three free surface effects: (1) net downward displacement of the bubble, caused by the impulsive interaction between bubble and pool surface, moved the contained aerosols away from the pool surface and made release during succeeding pulsations

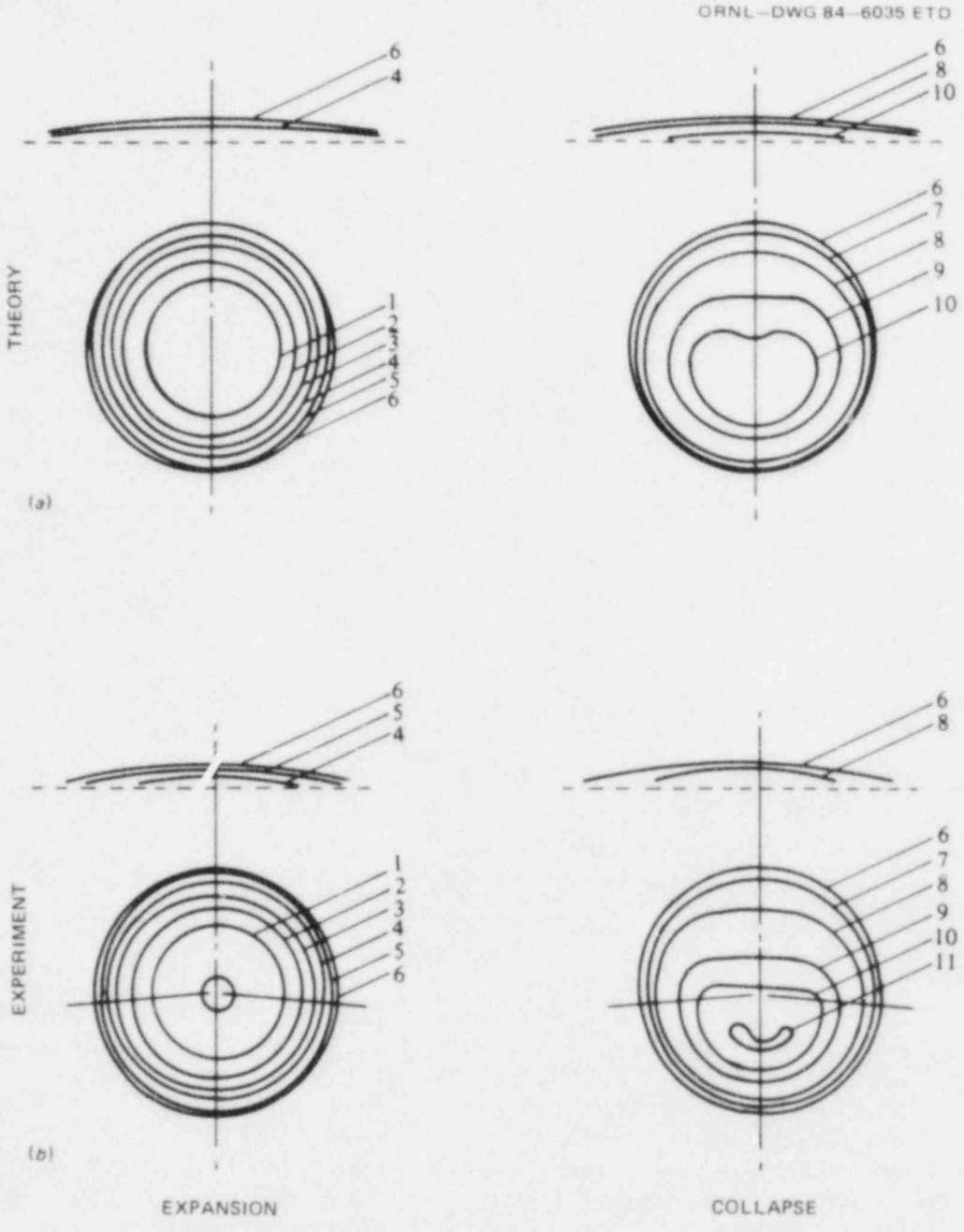

Fig. 22. Bubble and pool surface profiles following underwater vapor explosions ($\gamma = 1.68$). Contour numbers are indexed to advancing time (see source for description). *Source*: Reprinted with permission from J. R. Blake and D. C. Gibson, "Growth and Collapse of a Vapor Cavity Near a Free Surface," *Journal of Fluid Mechanics* 111, 123–40 (1981), Cambridge University Press.

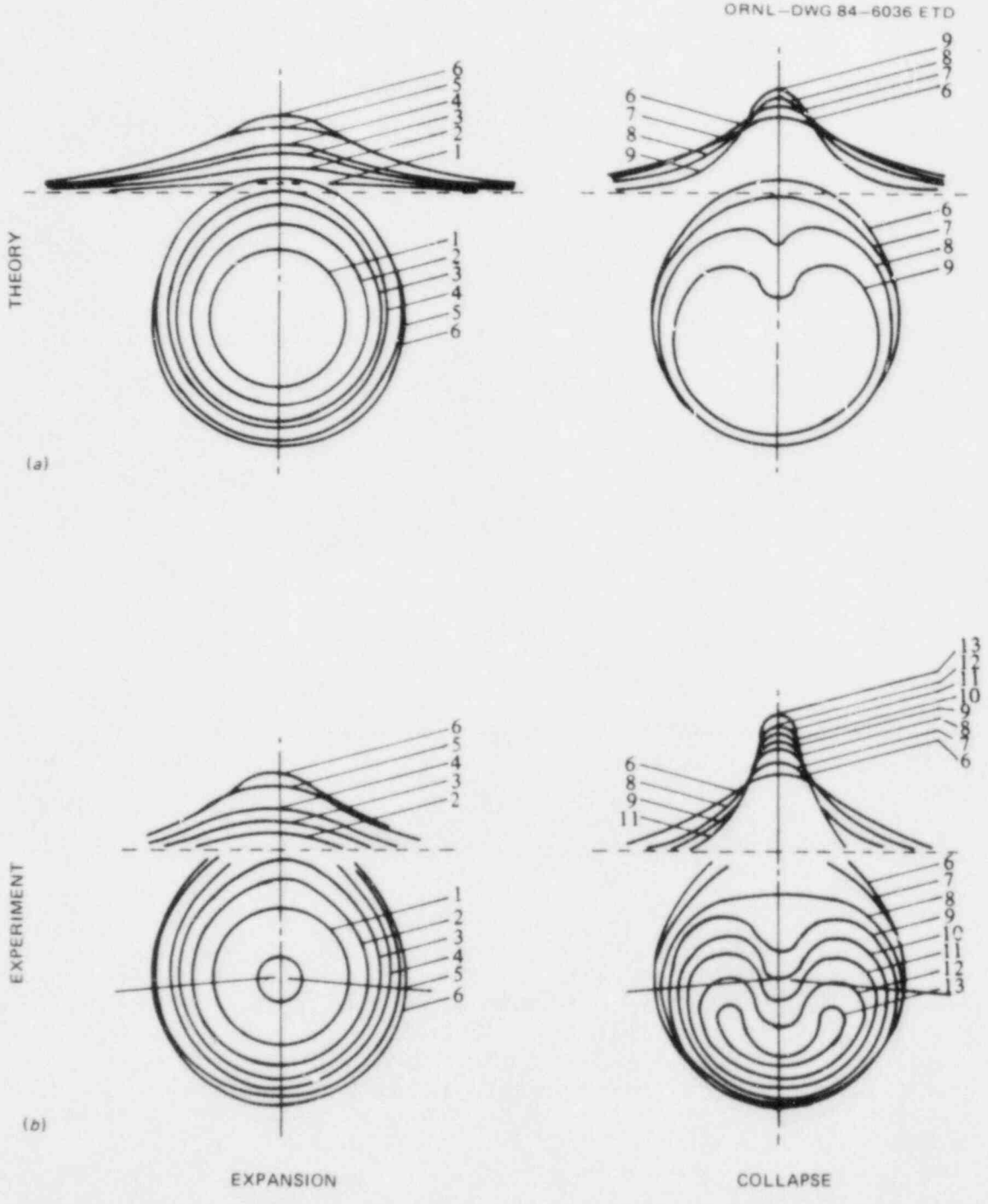

Fig. 23. Bubble and pool surface profiles following underwater vapor explosions (γ = 0.98). Contour numbers are indexed to advancing time (see source for description). *Source*: Reprinted with permission from J. R. Blake and D. C. Gibson, "Growth and Collapse of a Vapor Cavity Near a Free Surface," *Journal of Fluid Mechanics* 111, 123–40 (1981), Cambridge University Press.

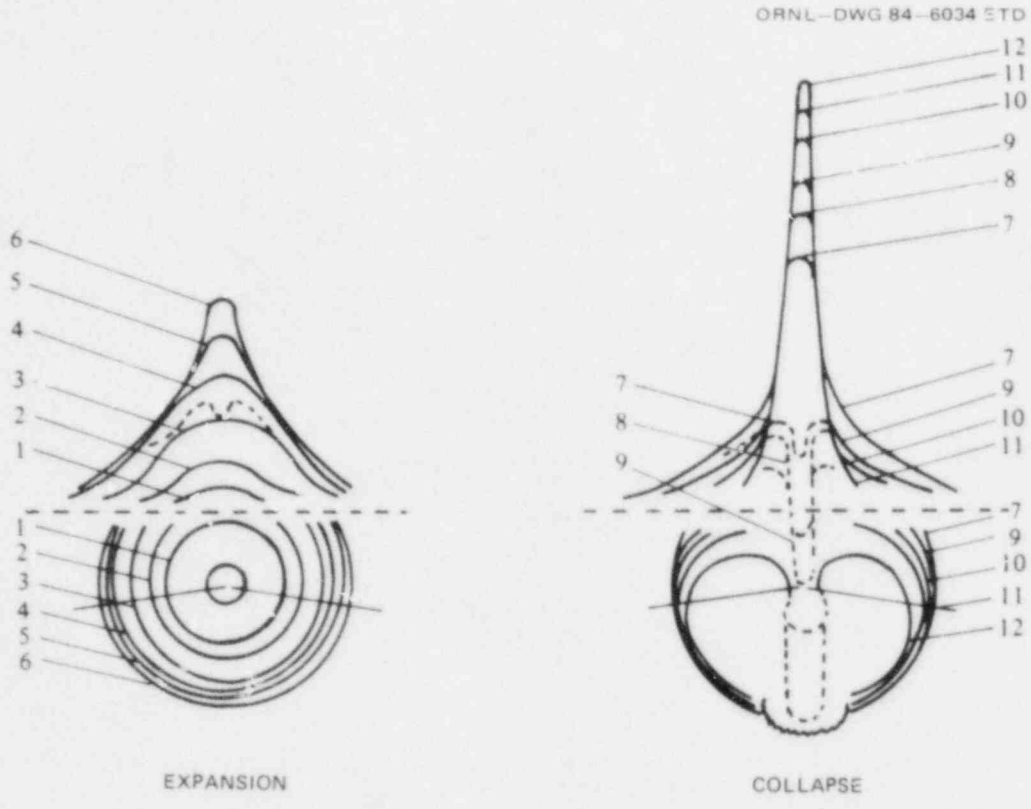

Fig. 24. Bubble and pool surface profiles following underwater vapor explosions (γ = 0.56). Contour numbers are indexed to advancing time (see source for description). *Source*: Reprinted with permission from J. R. Blake and D. C. Gibson, "Growth and Collapse of a Vapor Cavity Near a Free Surface," *Journal of Fluid Mechanics* 111, 123–40 (1981), Cambridge University Press.

less likely; (2) formation of a sodium finger or dome directly above the bubble enhanced the confinement of submerged bubbles and aerosols even when γ was considerably smaller than unity; and (3) bubble surface instabilities occurred earlier in the collapse phase of near-surface vapor explosions (FAST-108 and -109), with earlier breakup and downsizing probable. Along with bubble containment, these mechanisms supported the measured release in every experiment, except FAST-113 where more singular events occurred.

4.2.3 Aerosol release in FAST-113

Chemical analysis of aerosol samples indicated that contamination by sodium affected the release measurements in FAST-113. A 40-fold increase in sodium content was detected. The uranium content was small by comparison. These data are listed in Table 7, along with data from other experiments for which the likelihood of aerosol release was most comparable. The increase was confirmed by a postexperiment inspection that

ORNL PHOTO 0369-85

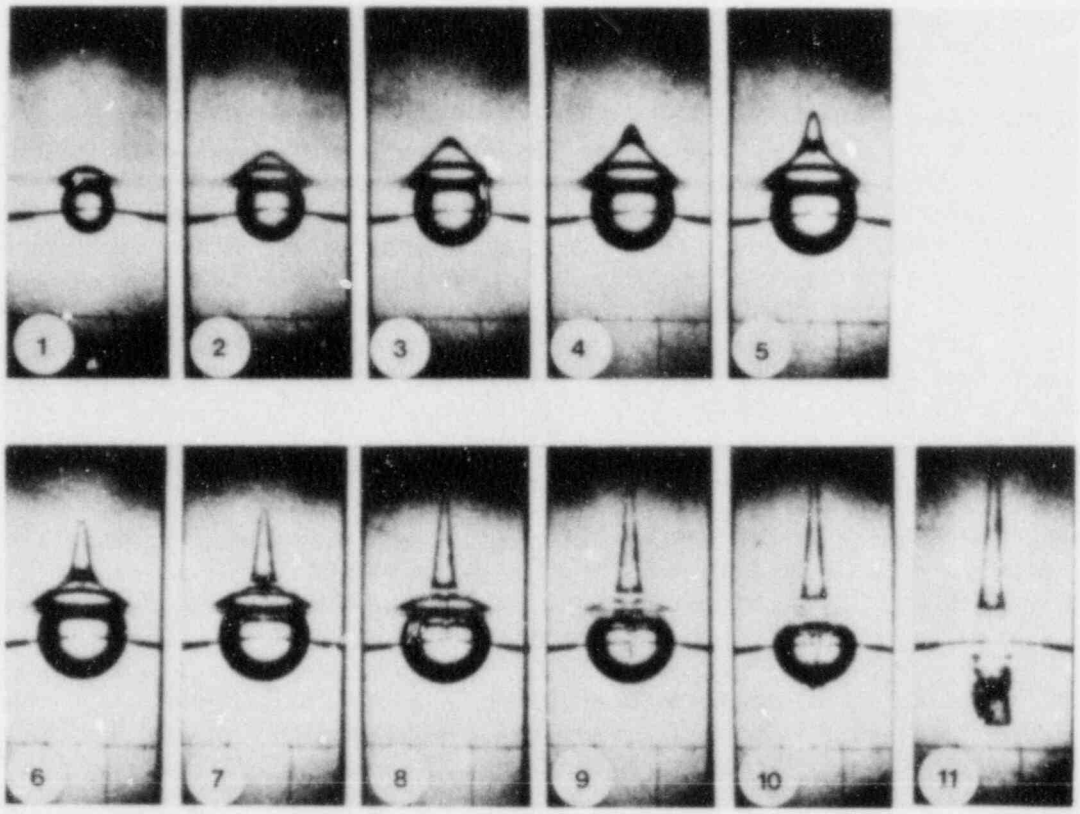

Fig. 25. High-speed photographs of bubble and pool surface during growth and collapse following a near-surface vapor explosion ($\gamma = 0.56$). *Source*: Reprinted with permission from J. R. Blake and D. C. Gibson, "Growth and Collapse of a Vapor Cavity Near a Free Surface," *Journal of Fluid Mechanics* 111, 123–40 (1981), Cambridge University Press. Photographed by Neil Hamilton.

Table 7. A comparison of chemical composition of aerosol samples collected in four experiments

Experiment No.	γ	Average sodium content (mg)	Average uranium concentration [(U(g)/Na(g)]
FAST-108	1.0	4.00	0.56×10^{-3}
FAST-109	1.1	5.95	0.20×10^{-3}
FAST-111		5.11	1.59
FAST-113	0.2	198.0	1.9×10^{-3}

revealed unusually thick deposits of sodium on the sampling equipment. This observation suggested that sodium had been dispersed from the pool and had splashed onto the upper internal surfaces of the vessel. The strength of the disturbance was attributed to the relatively low inertia of the upper pool layer and the relatively high CDV energy input (~37 kJ).*

Additional chemical analysis revealed that contamination by pool-borne UO_2 probably also occurred. The measured background mass concentration of UO_2 in the pool ($\sim 10^{-3}$) was roughly equivalent to the mass ratio of uranium-to-sodium detected on the aerosol filters (see Table 7). This suggested that the surface layer of sodium splashed and transported significant quantities of UO_2 to the cover gas, some of which impinged on sampling equipment, and that aerosol release was not as abundant as indicated by Figs. 17 and 20. Although an appropriate reduction in the release value could not be determined, analysis of pressure data indicated that significant release had occurred.

Significant release was inferred by comparing FAST-111 and FAST-113 pressure data. High-level "noise" in both cover gas pressure records was associated with turbulent mixing between cover gas and explosion products (including UO_2 aerosols). Although the noise levels were similar, onset was delayed ~25 ms in FAST-113 (see Figs. 14 and 16). Delay was attributed to bubble retention in the pool during the initial growth phase. Onset at 25 ms was attributed to venting of bubble contents into the cover gas; venting may have occurred near the first maximum. In addition, the flat, pool pressure trace (see Fig. 16) in conjunction with the observed cover gas noise indicated less coupling between pool and cover gas than in other undersodium experiments, consistent with a less confined bubble pulsation. More extensive bubble growth was expected in FAST-113 and was confirmed by bubble size measurements (see Table 5).

---

*A short-lived, pool surface displacement of +200 mm, at least 2 times larger than surface displacements in other experiments, was measured near the vessel wall.

5. SUMMARY

The preliminary analysis of experimental data has been completed; no additional work is planned. Conditions for aerosol release have been identified. Pool level was the most sensitive parameter affecting release. Consequently, pool-level settings spanned a wide range of values (−300 to +1060 mm) with increased selectivity at low, "positive" levels. Except for FAST-111 (300 mm oversodium) and FAST-113 (30 mm undersodium), measured release was extremely low: <1 mg or equivalently <0.006% of the original UO_2 sample. Pool surface effects impeded aerosol release in the low pool-level experiments.

Because aerosols were postulated to reside initially within the submerged bubble, the kinematics of the bubble were studied to determine whether the bubble vented into the cover gas. Cover gas pressure data were used to calculate an estimate of the maximum, multiphase bubble size. An indicator of aerosol release based on a bubble-size to pool-level ratio was proposed and was shown to be consistent with experimental observations. Pool pressure data were analyzed in light of theoretical models of bubble and pool dynamics to examine the role and nature of shock waves and dynamic pressures in FAST undersodium experiments. Differences between pool pressure and bubble pressure were attributed to the sodium flow within the pool. Results of computational simulations were also discussed; they supported the idea that fluid motions within the pool became more dynamic as the pool level decreased.

ACKNOWLEDGMENTS

The authors would like to identify those individuals who made special contributions to this report. C. V. Hardin, A. M. Smith, and W. A. Bird assisted with the operational aspects of the experiments. C. V. Hardin also helped provide the computer-generated plots of pressure data that appear in the report. Special thanks to R. J. Fox (Instrumentation and Controls Division, ORNL) for the digital interface used to process experimental data. D. B. Lloyd designed the liquid level probe used in FAST-113. R. E. Adams, N. C. Chen, U. Gat, R. E. MacPherson, and S. D. Rose reviewed the preliminary draft and suggested several improvements.

REFERENCES

1. A. W. Longest et al., "Source Term Experiments in FAST/CRI-III," pp. 3–16 in *Aerosol Release and Transport Program Quart. Prog. Rep. April–June 1983*, ed. R. E. Adams and M. L. Tobias, NUREG/CR-3422, Vol. 2 (ORNL/TM-8849/V2), Union Carbide Corp. Nuclear Div., Oak Ridge Natl. Lab., February 1984.

2. A. W. Longest et al., "Source Term Experiments in FAST/CRI-III," pp. 3–15 in *Aerosol Release and Transport Program Quart. Prog. Rep. July–September 1983*, ed. R. E. Adams and M. L. Tobias, NUREG/CR-3422, Vol. 3 (ORNL/TM-8849/V3), Martin Marietta Energy Systems, Inc., Oak Ridge Natl. Lab., April 1984.

3. A. W. Longest et al., "Source Term Experiments in FAST/CRI-III," pp. 3–23 in *Aerosol Release and Transport Program Semiann. Prog. Rep. October 1983–March 1984*, ed. R. E. Adams and M. L. Tobias, NUREG/CR-3830, Vol. 1 (ORNL/TM-9217/V1), Martin Marietta Energy Systems, Inc., Oak Ridge Natl. Lab., August 1984.

4. J. C. Petrykowski et al., "Source Term Experiments in FAST/CRI-III," pp. 3–12 in *Aerosol Release and Transport Program Semiann. Prog. Rep. April–September 1984*, ed. R. E. Adams and M. L. Tobias, NUREG/CR-3830, Vol. 2 (ORNL/TM-9217/V2), Martin Marietta Energy Systems, Inc., Oak Ridge Natl. Lab., February 1985.

5. T. S. Kress, G. W. Parker, and M. H. Fontana, *Work Plan: Transient Release from LMFBR Fuel*, ORNL/TM-4875, Union Carbide Corp. Nuclear Div., Oak Ridge Natl. Lab., September 1975.

6. A. L. Wright et al., *Fuel Aerosol Simulant Test Data Record Report: Argon Tests*, ORNL/NUREG/TM-365, Union Carbide Corp. Nuclear Div., Oak Ridge Natl. Lab., March 1980.

7. A. L. Wright et al., *Fuel Aerosol Simulant Test Data Record Report: Underwater Tests*, ORNL/TM-8085, Union Carbide Corp. Nuclear Div., Oak Ridge Natl. Lab., April 1982.

8. *Analysis of Hypothetical Core Disruptive Accident (HCDA)*, GEAP-13921, General Electric Company, December 1972.

9. M. J. Kelly, G. W. Parker, and J. M. Rochelle, *Development of the Capacitor Discharge Vaporization Technique to Produce Aerosols Formed under Conditions Postulated for Hypothetical Core Disruptive Accidents*, ORNL/NUREG/TM-160, Union Carbide Corp. Nuclear Div., Oak Ridge Natl. Lab., July 1978.

10. J. C. Petrykowski, A. L. Wright, and T. S. Kress, "LMFBR Fuel Vaporization Simulations in the FAST Facility," *Trans. Am. Nucl. Soc.* 45, 401 (1983).

11. A. L. Wright, A. M. Smith, and J. M. Rochelle, "Source Term Experiments in FAST/CRI-III," pp. 3–6 in *Aerosol Release and Transport Program Quart. Prog. Rep. October–December 1981*, ed. R. E. Adams and M. L. Tobias, ORNL/TM-8307, Union Carbide Corp. Nuclear Div., Oak Ridge Natl. Lab., May 1982.

12. K. Rush, J. M. Rochelle, and M. J. Kelly, *Power Regulator for Direct Heating of Material with Inverse Resistance-Temperature Properties*, ORNL/NUREG/TM-450, Union Carbide Corp. Nuclear Div., Oak Ridge Natl. Lab., June 1981.

13. A. L. Wright, unpublished notes, Chemical Technology Division, Oak Ridge Natl. Lab., 1979.

14. J. K. Fink, M. G. Chasanov, and L. Leibowitz, *Properties for Reactor Safety Analysis*, ANL-CEN-RSD-82-2, Argonne Natl. Lab., May 1982.

15. R. L. Webb, "Analysis of Large Two Phase Uranium Dioxide Bubble Behavior in Water and Sodium Pools," Ph.D. dissertation, University of Virginia, Charlottesville, 1984.

16. R. H. Cole, *Underwater Explosions*, Princeton University Press, Princeton, N.J., 1948.

17. J. W. Pritchett, *An Evaluation of Various Theoretical Models for Underwater Explosion Bubble Pulsations*, IRA-TR-2-71, Information Research Associates Inc., Berkeley, Calif., April 1971.

18. A. H. Shapiro, *The Dynamics and Thermodynamics of Compressible Flow*, Vol. 1, Ronald Press, New York, 1953.

19. G. B. Whitham, *Linear and Nonlinear Waves*, Wiley-Interscience, 1974.

20. J. R. Blake and P. Cerone, "A Note on the 'Impulse' Due to a Vapour Bubble Near a Boundary," *J. Aust. Math. Soc.* (Series B) 23, 383–93, 1982.

21. J. R. Blake and D. C. Gibson, "Growth and Collapse of a Vapor Cavity Near a Free Surface," *J. Fluid Mech.* 111, 123–40, 1981.

22. G. L. Chahine, "Interaction Between an Oscillating Bubble and a Free Surface," *J. Fluids Eng.* 99, 709–16, 1977.

23. M. S. Plesset, "Bubble Dynamics," pp. 1–18 in *Cavitation in Real Liquids*, ed. R. Davies, Elsevier Publishing Company, Amsterdam, 1964.

APPENDIX

DESCRIPTION OF UVABUBL II

UVABUBL-II is a thermal-hydraulic code that was developed by Webb and Reynolds[1] at the University of Virginia to interpret data collected from the FAST experiments. The code utilizes features of UVABUBL[2] and SAMPAC[3] to model bubble dynamics in an axisymmetric geometry and can be readily adapted to the FAST pressure vessel geometry. The code contains models of

1. radiation heat transfer between bubble and sodium,
2. mass transfer of sodium into bubble by surface vaporization and/or Rayleigh-Taylor surface instabilities,
3. UO_2 and sodium thermochemistry,
4. hydrodynamics of pool and bubble using the Marker-and-Cell method, and
5. real gas models of bubble contents and cover gas.

This code provides a means for detailed investigations of the dynamics of high-temperature uranium dioxide vapor bubbles under sodium for a wide range of conditions. Because many of the dynamics could not be measured experimentally, the code was a necessary adjunct to the test program. Ultimately, UVABUBL-II may be extended to analyze the bubble dynamics that could occur during a hypothetical hydrodynamic disassembly of an LMFBR core. The success of this application depends on the extent to which the code has been validated with existing experimental data. At this time, the FAST experiments are the sole source of this data.

References

1. R. L. Webb and A. B. Reynolds, "Use of 2-Dimensional SAMPAC Code for Constraint for Analysis of FAST Experiments in Bubble Behavior and Aerosol Conditions," in *LMFBR Core Disruptive Accidents Annual Report, October 1981–September 1982*, UVA/532345/NEEP83/101, University of Virginia.

2. D. R. Bradley, "Heat, Mass, and Momentum Transfer from Large Two-Phase Bubbles," Ph.D. dissertation, University of Virginia, Charlottesville, 1981.

3. S. S. Wang and J. H. Stuhmiller, "Analysis of Steam Chugging Phenomena," in *Vol. 3: SAMPAC Hydrodynamic Pool Response Code*, EPRI Fuel Report, Electric Power Research Institute, 1979.

NUREG/CR-4346
ORNL/TM-9479
Dist. Category R7

Internal Distribution

1-2.	R. E. Adams	18.	A. P. Malinauskas
3.	W. A. Bird	19-23.	J. C. Petrykowski
4.	J. R. Buchanan	24-26.	J. M. Rochelle
5.	R. J. Fox	27.	M. L. Tobias
6.	U. Gat	28.	H. E. Trammell
7.	J. A. Getsi	29.	G. D. Whitman
8.	C. V. Hardin	30-32.	A. L. Wright
9.	H. W. Hoffman	33.	ORNL Patent Office
10.	T. S. Kress	34.	Central Research Library
11.	D. B. Lloyd	35.	Document Reference Section
12-16.	A. W. Longest	36-37.	Laboratory Records Department
17.	R. E. MacPherson	38.	Laboratory Records (RC)

External Distribution

39. R. Curtis, Division of Accident Evaluation, Nuclear Regulatory Commission, Washington, DC 20555
40. R. L. Ritzman, Science Applications, Inc., 5 Palo Alto Square, Suite 2001, Palo Alto, CA 94304
41. M. Silberberg, Division of Accident Evaluation, Nuclear Regulatory Commission, Washington, DC 20555
42. J. Telford, Division of Accident Evaluation, Nuclear Regulatory Commission, Washington, DC 20555
43. T. Walker, Division of Accident Evaluation, Nuclear Regulatory Commission, Washington, DC 20555
44. D. H. Cho, Argonne National Laboratory, Bldg. 208, Argonne, IL 60439
45. A. B. Reynolds, Department of Nuclear Engineering and Engineering Physics, University of Virginia, Charlottesville, VA 22901
46. R. L. Webb, Savannah River Laboratory, E.I. Du Pont de Nemours Co., Aiken, SC 29801
47. P. M. Wood, Division of Accident Evaluation, Nuclear Regulatory Commission, Washington, DC 20555
48-49. Director, Office of Nuclear Regulatory Research, Nuclear Regulatory Commission, Washington, DC 20555
50. Office of Assistant Manager for Energy Research and Development, DOE, Oak Ridge Operations Office, Oak Ridge, TN 37831
51-52. Technical Information Center, DOE, Oak Ridge, TN 37831
53-302. Given distribution as shown in category R7 (NTIS-10)

NRC FORM 335 (2-84) NRCM 1102 3201, 3202

U.S. NUCLEAR REGULATORY COMMISSION

BIBLIOGRAPHIC DATA SHEET

SEE INSTRUCTIONS ON THE REVERSE

1. REPORT NUMBER (Assigned by TIDC, add Vol. No., if any)
NUREG/CR-4346
ORNL/TM-9479

2. TITLE AND SUBTITLE
Aerosol Release Experiments in the Fuel Aerosol Simulant Test Facility: Undersodium Experiments

3. LEAVE BLANK

4. DATE REPORT COMPLETED
MONTH: August YEAR: 1985

5. AUTHOR(S)
J. C. Petrykowski, A. W. Longest, J. M. Rochelle, A. L. Wright

6. DATE REPORT ISSUED
MONTH: September YEAR: 1985

7. PERFORMING ORGANIZATION NAME AND MAILING ADDRESS (Include Zip Code)
Oak Ridge National Laboratory
P.O. Box Y
Oak Ridge, Tennessee 37831

8. PROJECT/TASK/WORK UNIT NUMBER

9. FIN OR GRANT NUMBER
B0121

10. SPONSORING ORGANIZATION NAME AND MAILING ADDRESS (Include Zip Code)
Division of Accident Evaluation
Office of Nuclear Regulatory Research
U.S. Nuclear Regulatory Commission
Washington, DC 20555

11a. TYPE OF REPORT
Topical

b. PERIOD COVERED (Inclusive dates)

12. SUPPLEMENTARY NOTES

13. ABSTRACT (200 words or less)

The release of UO_2 aerosols from pools of sodium was studied in a series of ten experiments in the Fuel Aerosol Simulant Test (FAST) facility at Oak Ridge National Laboratory. The experiments were designed to provide a mechanistic basis for evaluating the radiological source term associated with a postulated, hypothetical core disruptive accident (HCDA) in a liquid metal fast breeder reactor (LMFBR). Aerosol was generated by capacitor discharge vaporization of UO_2 pellets which were submerged in a sodium pool under an argon cover gas. Measurements of the pool and cover gas pressures were used to study the transport of aerosol contained by vapor bubbles within the pool. Cover gas samples were filtered to determine the quantity of aerosol released from the pool. Trace amounts of UO_2 aerosol ($<0.3\%$ of the total pellet mass) were detected in the cover gas samples suggesting that the bulk of aerosol was trapped within bubbles confined by the pool. The report contains (1) a description of the experiments, (2) data records for the pool pressure, the cover gas pressure, and the UO_2 aerosol concentration in the cover gas and, (3) an analysis of the experimental findings using simplified models of bubble behavior.

14. DOCUMENT ANALYSIS - a. KEYWORDS/DESCRIPTORS
Liquid Metal Cooled Reactors
Fast Reactors
Aerosols

b. IDENTIFIERS/OPEN-ENDED TERMS
Radioactive Aerosols
Sodium Cooled Reactors
Energetic Core Disruptive Accidents
LMFBR Source Term
Capacitor Discharge Vaporization Experiments

15. AVAILABILITY STATEMENT
Unlimited

16. SECURITY CLASSIFICATION
(This page) Unclassified
(This report) Unclassified

17. NUMBER OF PAGES

18. PRICE